

PROCESSING OF ZrB_2 - ZrC - Zr_xSi_y CERAMIC BY REACTIVE METAL
PENETRATION

NISCHEL B. MAHESWARAIAH

Department of Mechanical Engineering

APPROVED:

Arturo Bronson, Ph.D., Chair

John F. Chessa, Ph.D.

Felicia S. Manciu, Ph.D.

Patricia D. Witherspoon, Ph.D.

Dean of the Graduate School

Copyright ©

by

Nischel B. Maheswaraiah

2010

PROCESSING OF ZrB_2 - ZrC - Zr_xSi_y CERAMIC BY REACTIVE METAL
PENETRATION

by

NISCHEL B. MAHESWARAIAH, B.E.M.E.

THESIS

Presented to the Faculty of the Graduate School of

The University of Texas at El Paso

in Partial Fulfillment

of the Requirements

for the Degree of

MASTER OF SCIENCE

Department of Mechanical Engineering

THE UNIVERSITY OF TEXAS AT EL PASO

May 2010

UMI Number: 1477805

All rights reserved

INFORMATION TO ALL USERS

The quality of this reproduction is dependent upon the quality of the copy submitted.

In the unlikely event that the author did not send a complete manuscript and there are missing pages, these will be noted. Also, if material had to be removed, a note will indicate the deletion.



UMI 1477805

Copyright 2010 by ProQuest LLC.

All rights reserved. This edition of the work is protected against unauthorized copying under Title 17, United States Code.



ProQuest LLC
789 East Eisenhower Parkway
P.O. Box 1346
Ann Arbor, MI 48106-1346

ACKNOWLEDGEMENTS

I would like to express my sincere gratitude to my advisor, Dr. Arturo Bronson, for his guidance and encouragement during my time at University of Texas at El Paso. Many times, his insight and incredible intuition helped me to find the right direction in my research.

I am grateful to Dr. Jack Chessa and Dr. Felicia Manciu for their time being on the committee and thoughtful suggestions. I would like to thank Dr. Chintalapalle Ramana for his teachings on scanning electron microscope. I also thank Air Force of Scientific Research (AFOSR) for funding the project. I also want to thank all my teachers in the mechanical engineering department.

I would like to thank my friends at university of Texas at El Paso: Alvaro Sandate, Vishwanath Ardha, Carlos Castillo, Mario Ruvalcaba, David Pham, and Brenda Mota. This group has been a constant source of advice, support and laughs. They have been outstanding colleagues, and I am honored to also call them my friends.

Finally, this dissertation is dedicated to my parents and brother. Their encouragement and support has enabled me to push on through the toughest of times. I could never thank them enough for all that they have done for me. I am forever grateful.

ABSTRACT

The processing of $ZrB_2-ZrC-Zr_xSi_y$ composite by reactive metal penetration was investigated as a successor to the ZrB_2-SiC composites for hypersonic vehicles application, which cannot be used for extended time at temperatures greater than $1600^\circ C$ due to formation of SiO and CO gases. Zirconium (Zr), zirconium disilicide ($ZrSi_2$), and boron carbide (B_4C) were reacted in graphite crucibles for 60, 120, 180, and 240 minutes. Microscopy and x-ray diffraction (XRD) deduced the formation of a heterogeneous microstructure of $ZrB_2-ZrC-Zr_xSi_y$ precipitates surrounded by a solidified Zr-Si melt. Unreacted boron carbide was observed in samples held at $1860^\circ C$ for 60 minutes and 120 minutes, so thermodynamic equilibrium was not achieved. The reaction for the composite formation is as follows:



The most consistent microstructures were seen on the samples heated for 180 minutes and 240 minutes, in which the free B_4C completely decomposed to zirconium boride and carbide. Also, because of the closeness of the initial compositions of Zr and Si (12 wt% and 14 wt%) on the Zr-Si phase diagram, there was not much difference in the final phases obtained in both compositions.

TABLE OF CONTENTS

ACKNOWLEDGEMENTS.....	iv
ABSTRACT	v
Chapter 1: INTRODUCTION	1
1.1: Overview of Ultra-High Temperature Ceramics.....	1
1.2: Research Objective	2
Chapter 2: LITERATURE REVIEW	4
2.1: Processing of Ultra-High Temperature Ceramics.....	4
2.1.1: Reactive Metal Penetration.....	4
2.2: Phase Diagrams	6
2.2.1: Zr-Si Phase Diagram	6
2.2.2: B-C-Zr Phase Diagram	9
2.2.3: Zr-B ₄ C-ZrSi ₂ Phase Diagram	9
2.3: Oxidation of ultra-high temperature ceramic	13
2.3.1 Zr-Si-O Phase Diagram	13
2.3.2 ZrO ₂ -SiO ₂ Phase Diagram	14
Chapter 3: RESEARCH METHODOLOGY.....	17
3.1: Sample Preparation.....	17
3.2: Experimental Procedure	18
3.3: Microstructure Characterization.....	19
Chapter 4: RESULTS	26

4.3: Results Summary	27
Chapter 5: DISCUSSION.....	45
5.1: Oxygen Potential Reduction within the graphite Enclosure.....	45
5.2: Phase Relations between Zr/B ₄ C/Si	45
5.4: Microstructures	47
Chapter 6: CONCLUSION.....	52
REFERENCES	53
CURRICULUM VITA	56

LIST OF FIGURES

Figure 2.1: Ellingham Diagram for Carbides [Outotec].	7
Figure 2.2: Zr-Si Phase Diagram in mole fraction. The red arrows indicate the starting Zr-Si liquid compositions [Okamoto-1996].	8
Figure 2.3: B-C-Zr Ternary Phase Diagram at 1800°C [Outotec].	10
Figure 2.4: B-C-Zr Ternary Phase Diagram at 2400°C [Outotec].	11
Figure 2.5: Zr-B ₄ C-ZrSi ₂ Pseudo-Ternary Phase Diagram at 1860°C [FactSage].	12
Figure 2.6: FEA model of the ZrB ₂ -ZrC-Zr Composite with Oxide Scales [Petla-2010].	14
Figure 2.7: Zr-Si-O Ternary Phase Diagram at 1680°C [Sorrell-1986].	15
Figure 2.8: ZrO ₂ -SiO ₂ Pseudo-Binary Phase Diagram [Kaiser-2008].	16
Figure 3.1: Sample Setup.	17
Figure 3.2: Graphite Enclosure Setup.	20
Figure 3.3: Graphite Enclosure with Graphite Crucible Sample.	21
Figure 3.4: Cross-section of the Graphite Enclosure.	22
Figure 3.5: Reaction Tube Setup.	23
Figure 3.7: Reaction Tube Cap.	24
Figure 3.8: Cooling Jacket.	24
Figure 3.6: Quartz Reaction Tube.	24
Figure 3.9: Bottom Reaction Tube Cap.	25
Figure 3.10: Cooling Jacket Cap.	25
Figure 4.1: Cross-section of a processed sample showing the effect of the levitation caused by the magnetic field of the induction furnace.	28

Figure 4.2: XRD diagram for Zr-12wt%Si held at 1860°C for 60 minutes.....	29
Figure 4.3: XRD diagram for Zr-16wt%Si held at 1860°C for 60 minutes.....	30
Figure 4.4: XRD diagram for Zr-12wt%Si held at 1860°C for 120 minutes.....	31
Figure 4.5: XRD diagram for Zr-16wt%Si held at 1860°C for 120 minutes.....	32
Figure 4.6: XRD diagram for Zr-12wt%Si held at 1860°C for 180 minutes.....	33
Figure 4.7: XRD diagram for Zr-16wt%Si held at 1860°C for 180 minutes.....	34
Figure 4.8: XRD diagram for Zr-12wt%Si held at 1860°C for 240 minutes.....	35
Figure 4.9: XRD diagram for Zr-16wt%Si held at 1860°C for 240 minutes.....	36
Figure 4.10: SEM Micrograph of ZrB ₂ -ZrC precipitates surrounded by solidified Zr-Si melt and the unreacted B ₄ C in sample held at 1860°C for 60 minutes.....	37
Figure 4.11: Micrograph of ZrB ₂ -ZrC precipitates surrounded by solidified Zr-Si melt and the unreacted B ₄ C in sample held at 1860°C for 60 minutes.	38
Figure 4.12: Micrograph with a closer look at the unreacted B ₄ C and ZrB ₂ -ZrC-Zr _x Si _y precipitates in sample held at 1860°C for 60 minutes.	39
Figure 4.13: Micrograph of ZrB ₂ -ZrC-Zr _x Si _y precipitates encased within solidified Zr-Si melt in a sample held at 1860°C for 120 minutes.....	40
Figure 4.14: Micrograph with a closer look at the unreacted B ₄ C and ZrB ₂ -ZrC-Zr _x Si _y precipitates in sample held at 1860°C for 120 minutes.	41
Figure 4.15: Micrograph of ZrB ₂ -ZrC precipitates encased within solidified Zr-Si melt in a sample held at 1860°C for 180 minutes.	42
Figure 4.16: Micrograph of ZrB ₂ -ZrC precipitates in a completely reacted sample held at 1860°C for 180 minutes.	43

Figure 4.17: Micrograph with ZrB_2 - ZrC precipitates in a completely reacted sample held at 1860°C for 240 minutes.	44
Figure 5.1: Ellingham Diagram for oxides.	48
Figure 5.2: Zr-B ₄ C-Si Pseudo-Ternary Phase Diagram at 1900°C.	49
Figure 5.3: Zr-B ₄ C-Si Pseudo-Ternary Phase Diagram at 2400°C.	50
Figure 5.4: Ellingham Diagram for Zirconium Silicides.	51

Chapter 1: INTRODUCTION

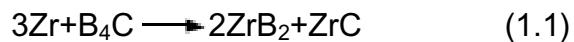
1.1: Overview of Ultra-High Temperature Ceramics

The wing leading edge and nose caps of the hypersonic vehicles are subjected to temperatures greater than 2000°C during their reentry and sustain severe conditions caused by vaporization, erosion and oxidation. In addition to chemical reactivity, the durability of materials to ultrahigh temperatures (>1600°C) causes severe mechanical interaction resulting from thermal shock for ceramic materials as they cycle from room temperature to the extreme temperatures. The composites must then sustain a synergistic effect contributed from the chemical and mechanical interactions at ultrahigh temperatures exposure, requiring selection of the optimal material system.

The carbides and borides of the transition metals (e.g., ZrC, HfC, ZrB₂ and HfB₂) have been suggested as materials for ultrahigh temperature ceramics [Opeka-2004, Bronson-1992], because of their exceptionally high melting temperatures of greater than 3000°C. The other important distinctive qualities are solid-state stability, good thermomechanical properties, and high mechanical properties, values as shown in table 1.1. However, a scale must protect the foregoing carbides and borides, which readily react with oxygen. Various researchers [Hinze-1975, Karlsdottir-2007, Fahrenholtz - 2007, and Monteverde-2007] determined through their meticulous study that the ZrB₂-SiC system is protected from oxidation because an adherent silicate scale forms and decreases significantly the diffusion of oxygen into the substrate. However, the formation of SiO and CO limits the operational temperature of SiC because the CO forms along the SiC/ SiO₂ interface as well as SiO (g) creates a bubbling action at

temperatures greater than 1600 -1700°C [Levine-2002, Bronson -2008,]. Hence, a silicide must be found without the formation of gaseous products though still with the protective properties of a silicate layer, which lowers the oxygen diffusion.

An additional drawback of ultrahigh temperature materials is their processing because the systems require ultrahigh temperatures, controlled porosity and significantly low impurities. For example, ZrB₂ and ZrC have melting points of 3244°C [Okamoto-1993] and 3427°C [Okamoto-1996], respectively, but SiO₂ impurities coalescing in the grain boundaries would lower the yield strength. Johnson et al. [6] developed a technique of reacting liquid Zr with a packed bed of B₄C, the process called reactive metal penetration. As the Zr penetrates the packed bed, the following reaction ensues exothermically with the Gibbs free energy of formation at 1855 °C, ΔG = - 673 kJ:



An additional contribution would be to use a Zr -Si melt instead of Zr melt to create a boride/carbide precipitates embedded in a Zr -Si alloy matrix. Upon oxidation, the Si would react to form a silicated layer.

1.2: Research Objective

The research investigates the processing of a ceramic composite consisting of ZrB₂, ZrC, Zr_xSi_y precipitates within a metal matrix of Zr -Si alloy. The objective of the research was to determine the extent of the silicide precipitation as the Zr -Si liquid penetrates the B₄C packed bed. The original Zr-Si liquid corresponded to the Zr-12 wt% Si, which lies within the Zr₃Si-ZrSi two-phase region and Zr-16 wt% Si, which lies within the Zr₂Si-Zr₃Si₂ region of the Zr -Si phase diagram . The Zr_xSi_y would ultimately form a

protective SiO_2 and ZrO_2 scales to provide oxidation resistance to the composite. The liquid SiO_2 embedded in the ZrO_2 scales fills up the cracks resulting in stress reduction. The study investigated the processing $\text{ZrB}_2\text{-ZrC-Zr}_x\text{Si}_y$ composite by reactive metal penetration and its dependence on time.

Table 1.1: Properties of Borides and Carbides [Okamoto-1993, Okamoto-1996, Samsonov-1980]

Material	Melting Temperature (°C)	Thermal Expansion Co-efficient (10^{-6} C^{-1})	Flexural Strength (MPa)	Young's Modulus (GPa)	Density (g/cm^3)
ZrB_2	3244	6.2	351	489	6.1
ZrC	3427	7.1	323	390	6.7
HfB_2	3250	6.5	340	530	11.2
HfC	3890	7.1	150	424	12.7
SiC	2545	4	596	448	3.22

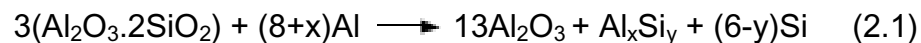
Chapter 2: LITERATURE REVIEW

2.1: Processing of Ultra-High Temperature Ceramics

There are several methods of processing ultra-high temperature ceramics (UHTC) though reactive metal penetration is an economical and uncomplicated technique of creating interconnecting precipitates in a metal/ceramic composite, without hot pressing. For considering systems suitable for reactive metal penetration, the thermodynamic reactions and thermodynamic compatibility of phases must be determined [Fahrenholtz-2006]. The reactions should be thermodynamically favorable which refers to the Gibb's free energy of reaction, as shown in figure 2.1. The Gibbs free energy of ZrC is considerably less than B₄C and the liquid would displace the boron via the reaction shown in equation 1.1. The phase equilibria must then be checked with phase diagrams, if available.

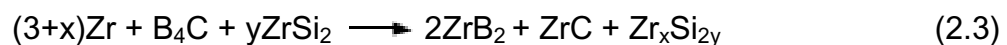
2.1.1: Reactive Metal Penetration

Tomsia et al. [5] and Johnson et al. [6] have used reactive metal penetration to form a composite by capitalizing on interfacial reaction between a metal and ceramic. Tomsia et al. [5] reacted molten aluminum with mullite to form Al₂O₃ with Al-Si alloy. The liquid aluminum penetrated the silicate preform dissolving SiO₂ and forming Al₂O₃ at the reaction layer. The process continues with oxygen diffusing through the initial Al₂O₃ product and reacting with molten aluminum forming more Al₂O₃. The dissolved Si moves away from the reaction zone forming Al-Si alloy.



Similarly, Johnson et al. [6] reported that molten zirconium infiltrated through the open porosity of B₄C reacting to form simultaneously precipitates of ZrB₂ and ZrC. The dissolution of B₄C results in a thin boron-rich zirconium alloy. The boron-rich zirconium alloy pulls down the previously formed ZrB₂-ZrC layer by transportation phenomena and at the same time, reacting to leave behind a ZrB₂-ZrC-Zr composite. Liquid metal can infuse into a ceramic preform by creating a pressure difference between the outer wall and inner core as aluminum or zirconium penetrating the ceramic preforms of mullite (3Al₂O₃.2SiO₂), SiO₂ or B₄C [Bronson-1997]. For ceramics with low open porosity, Odegard and Bronson considered capillary motion driven by surface tension instead of pressure difference for transporting the liquid metal with the reaction shown in equation 1.1.

For the ZrB₂-ZrC-Zr_xSi_y system, with the addition of ZrSi₂ to the initial constituents, the Zr serves as a carrier for Si when liquid Zr-Si penetrates into a preform. Zirconium silicides form upon cooling and their composition depends on the initial zirconium and zirconium disilicides. The reaction occurs very fast with linear kinetics with a rate constant between 1.6×10⁻² and 3.9×10⁻² cm²/s [Tomsia-1999, Johnson-1991]. Initially, the rate-determining step will be the interfacial reaction between Zr-Si melt and boron carbide. Once the reaction initiates, the boron carbide-liquid Zr-Si reaction will be faster than the diffusion of Si, B and C [Johnson-1991, Lu-1999, Tomsia-1999, Fahrenholtz-2006,].



2.2: Phase Diagrams

2.2.1: Zr-Si Phase Diagram

The Zr-Si phase diagram gives the phase equilibria with a maximum melting at 2250°C for Zr_5Si_4 compound, as shown in figure 2.2. The melting temperatures of Si and Zr are 1414 °C and 1855 °C respectively. Eutectic reactions occur on either side of binary - at 1370°C in the Si-rich region (10 at% Zr) and at 1570 °C in the Zr-rich region (91.2 at % Zr). The maximum solubility of Si in Zr is less than 1 at % Si (due to the relatively large size of Zr atom) forming Zr (body centered cubic, BCC) and Zr (hexagonal close packed, HCP), but Zr is not soluble in Si. The Zr -Si system has the following intermetallic compounds: $ZrSi_2$, $ZrSi$ and $ZrSi$, Zr_5Si_4 and Zr_5Si_4 , Zr_3Si_2 , Zr_5Si_3 , Zr_2Si and Zr_3Si . The $ZrSi_2$ (33 at% Zr) phase initially forms at 1620 °C with a peritectic transformation of liquid and $ZrSi$. Similarly, $ZrSi$ forms from the peritectic reaction of liquid and Zr_5Si_4 at 2210 °C though $ZrSi$ structure changes at 1460 °C. Polymorphic transformations also occur at 1860 °C for Zr_5Si_4 and Zr_3Si_2 . The Zr_5Si_4 undergoes a congruent transformation at 2210 °C. The peritectic formation of Zr_3Si_2 (60 at% Zr) occurs at 2215°C. The Zr_5Si_3 (62.5 at% Zr) also forms peritectically, but transforms with a eutectoid reaction at 1745 °C forming Zr_2Si and Zr_3Si_2 when cooled slowly. The Zr_5Si_3 is thermodynamically unstable at temperatures less than 1745 °C as indicated by the Zr-Si phase diagram. The incongruent reactions of Zr_2Si and Zr_3Si occur at 1925°C and 1650°C respectively.

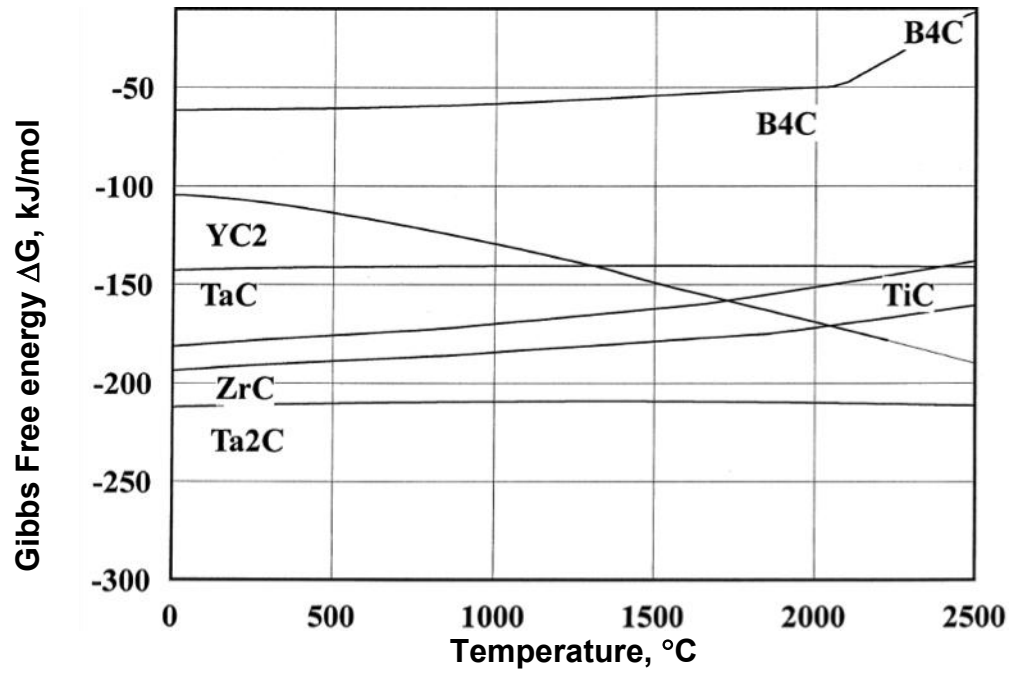


Figure 2.1: Ellingham Diagram for Carbides [Outotec].

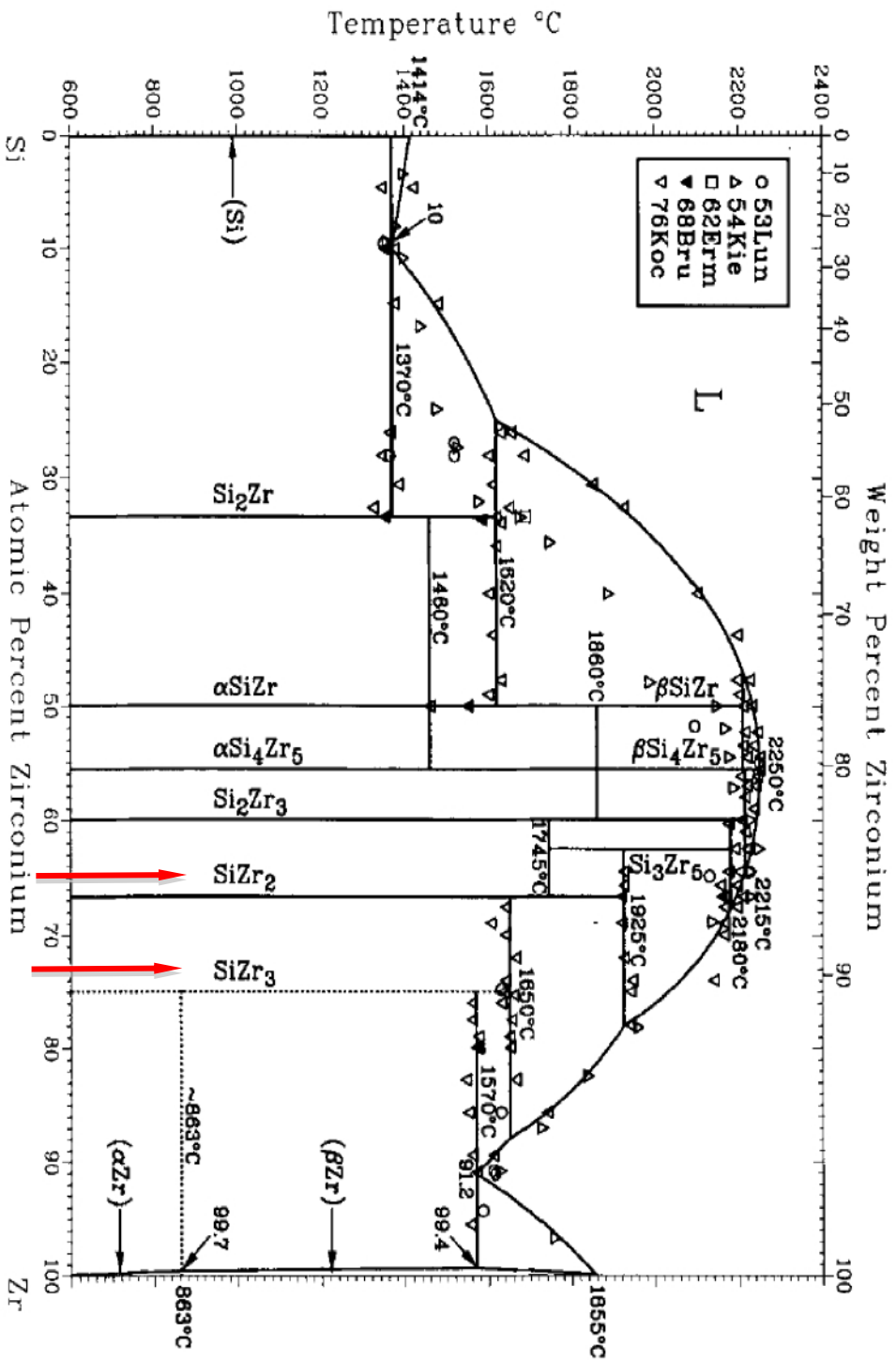


Figure 2.2: Zr-Si Phase Diagram in mole fraction. The red arrows indicate the starting Zr-Si liquid compositions [Okamoto-1996].

2.2.2: B-C-Zr Phase Diagram

Isothermal sections of Zr-B-C system at temperatures, 1800 °C and 2400 °C are shown in figures 2.3 and 2.4. For the isothermal section at 1800°C, we observe four binary compounds, ZrB₂, ZrC, B₄C, and ZrB₁₂; and the three-phase field, ZrB₂+ZrC+LIQUID forms. The phase diagram shows no other liquid present apart from the unreacted molten zirconium. The three-phase field (ZrB₂+ZrC+LIQUID) is a product of molten Zr reacting with B₄C. Phase layers such as ZrC+B₄C and ZrC+B₄C+C are also present at 1800 °C. At 2400 °C, boron-rich liquid exists due to the peritectic melting of ZrB₁₂ at 2030°C and eutectic reaction between ZrB₂, B₄C, and C at 2165°C. The Zr-rich liquid region grows larger at 2400 °C due to the decomposition of some of the ZrB₂+ZrC+LIQUID phase.

2.2.3: Zr-B₄C-ZrSi₂ Phase Diagram

The pseudo-ternary system at 1860 °C shown in figures 2.5 contains three zirconium silicides, ZrSi, Zr₂Si and Zr₅Si₃; boride, ZrB₂; and carbide, ZrC. The FactSage database, which generated the phase diagram, does not consider the other silicide intermetallics from the Zr-Si phase diagram such as Zr₅Si₄, Zr₃Si₂ and Zr₃Si. Zr and ZrSi₂ melt to form Zr-Si liquid, which then reacts with B₄C leaving behind a composite of ZrB₂, ZrC and Zr_xSi_y, given sufficient time. The stable phases ZrB₂ and ZrC are in equilibrium with ZrSi and Zr₅Si₃ between 30 at% ZrSi₂ and 5 at% ZrSi₂. The compound SiB₁₄ is formed by the reaction between B₄C and SiB₆.

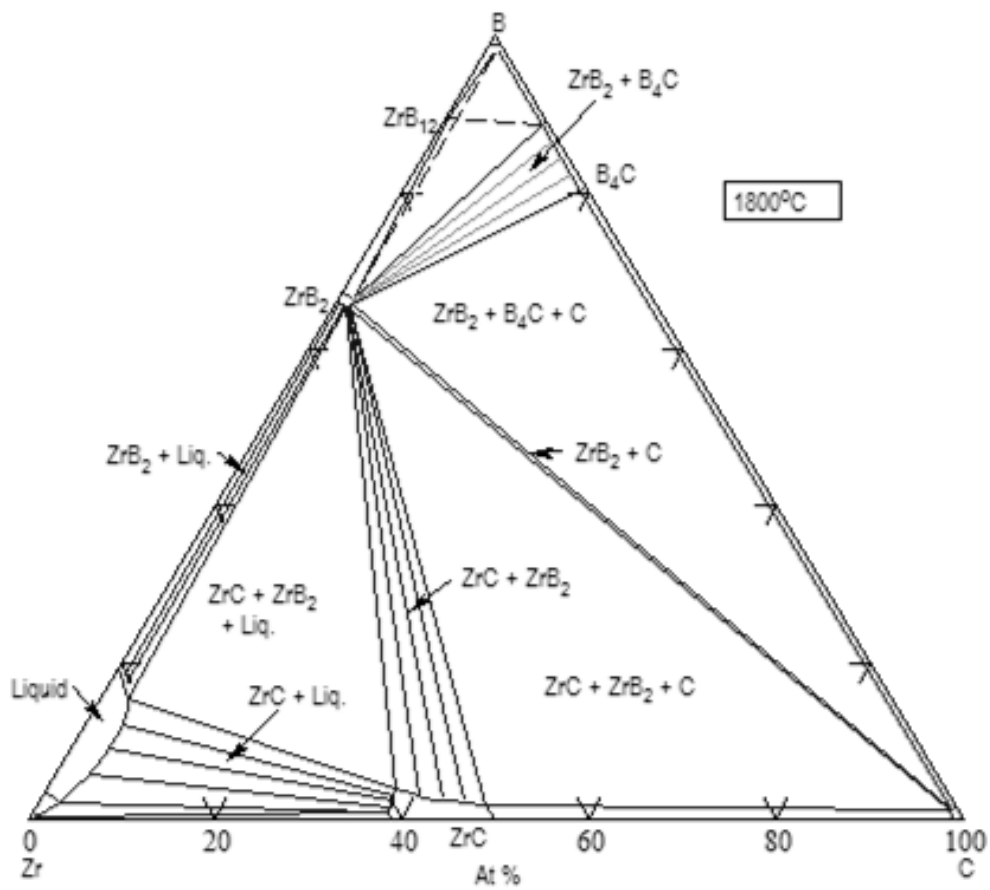


Figure 2.3: B-C-Zr Ternary Phase Diagram at 1800°C [Outotec].

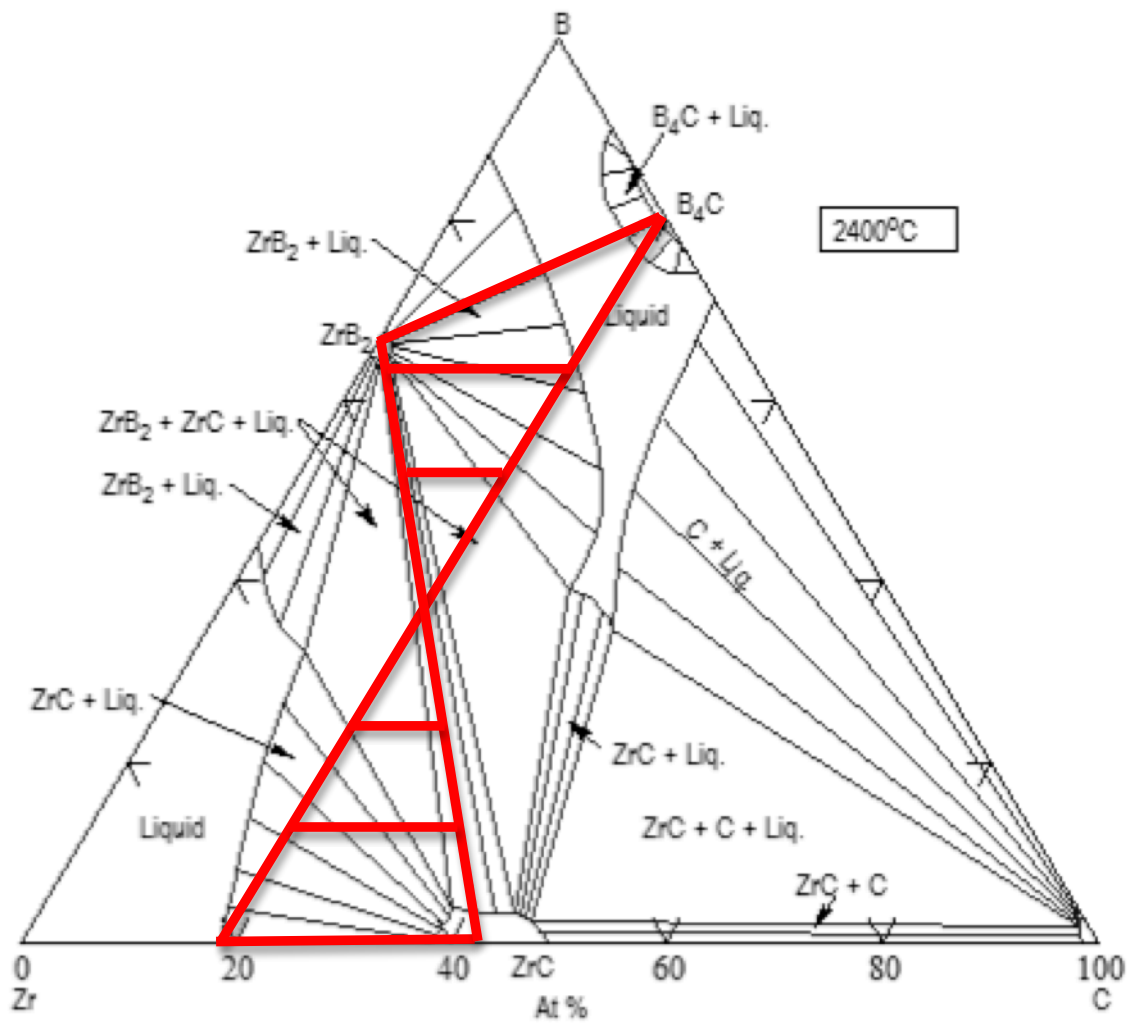


Figure 2.4: B-C-Zr Ternary Phase Diagram at 2400°C [Outotec].

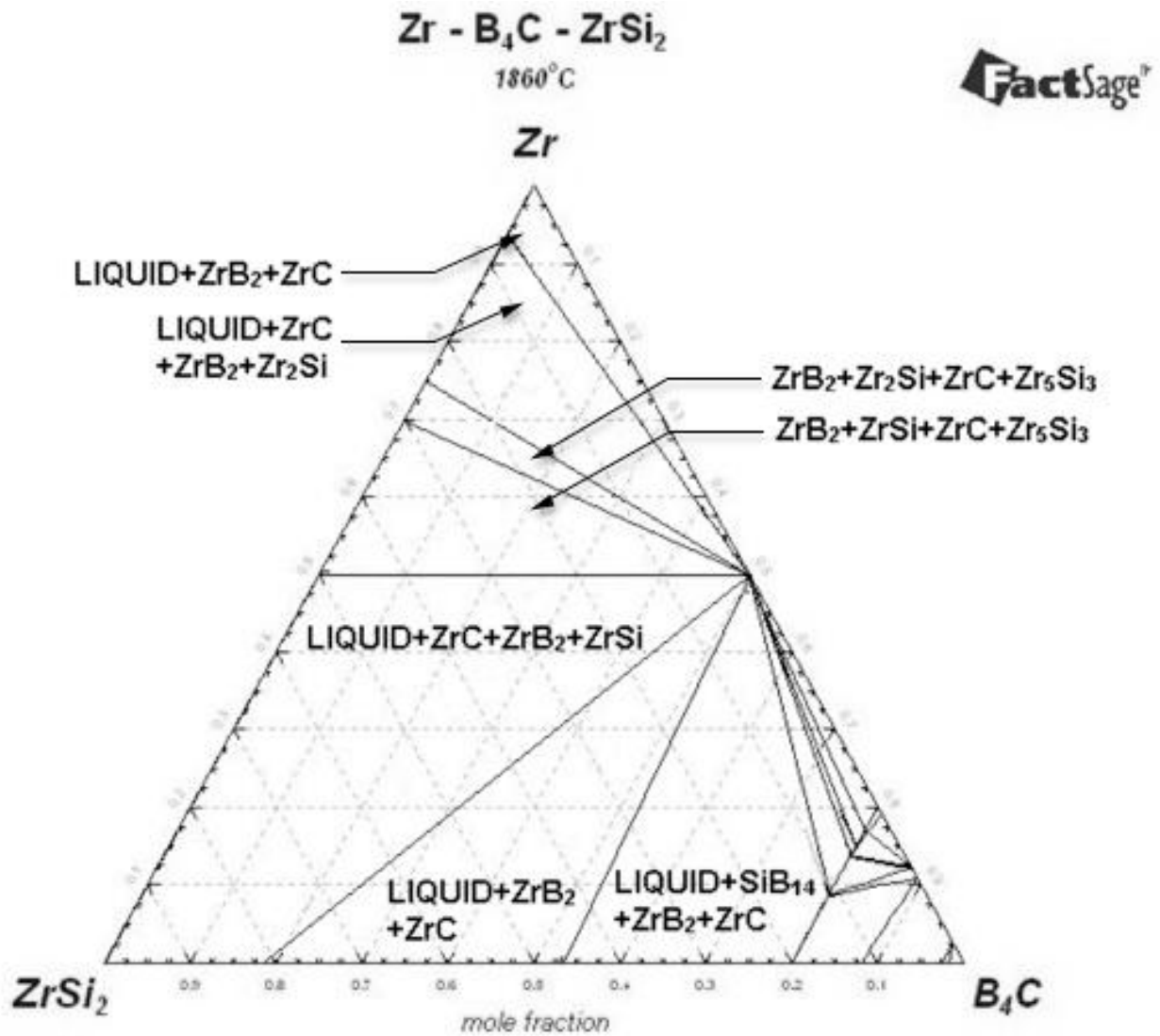


Figure 2.5: Zr-B₄C-ZrSi₂ Pseudo-Ternary Phase Diagram at 1860°C [FactSage].

2.3: Oxidation of ultra-high temperature ceramic

Transition Metal (Zr, Hf, Ti and Ta) diborides and carbides are more suitable for use as ultra-high temperature ceramics (UHTC) because of their oxidation resistance by forming scales, thereby, reducing oxygen ingress [Opeka-2004, Fahrenholtz-2007]. The oxidation resistance of borides and carbides can be increased by the addition of Si, which form a protective SiO_2 layer [Hinze-1975]. Researchers have reported the formation of multi-layer oxide scale upon oxidation of ZrB_2 -SiC composite at temperatures greater than 1500 °C [Hinze-1975, Karlsdottir -2007, Fahrenholtz-2007, Monteverde-2007]. Up to 1200°C, the liquid SiO_2 - B_2O_3 protects the composite by preventing oxygen diffusion and preventing scale spallation. At temperatures greater than 1200°C, the boron vaporizes from the outer borosilicate scale and completely at around 1500°C leaving behind an outer amorphous silica-rich scale with ZrO_2 precipitates covering a zirconia-rich scale with SiO_2 precipitates. This layered oxide scales are capable of extremely high temperature oxidation resistance due to the viscosity and wettability of SiO_2 glass layer. The diffusion of oxygen through the liquid SiO_2 layer is the rate-determining step and shows parabolic oxide scale growth rate. A simulated ZrO_2 - SiO_2 scale on a ZrB_2 -ZrC-Zr composite is shown in figure 2.6.

2.3.1 Zr-Si-O Phase Diagram

From the Zr-Si-O ternary phase diagram shown in figure 2.7, the equilibrium phases, which must be present at 1680 °C, are ZrO_2 (solid), SiO_2 (liquid) and ZrSiO_4 . A discrepancy exists in this phase diagram as ZrSiO_4 is shown to be present even though the pseudo-binary ZrO_2 - SiO_2 phase diagram (figure 2.8) suggests dissociation of ZrSiO_4

the pseudo-binary ZrO_2 - SiO_2 phase diagram (figure 2.8) suggests dissociation of $ZrSiO_4$ at $1673^\circ C$. The ZrO_2 - $ZrSi_2$ tie line prevents other silicides from equilibrating with SiO_2 and $ZrSiO_4$.

2.3.2 ZrO_2 - SiO_2 Phase Diagram

The pseudo-binary phase diagram of ZrO_2 - SiO_2 in figure 2.8 shows compound Zircon ($ZrSiO_4$), which decomposes in solid state at $1673^\circ C$ into solids, ZrO_2 and SiO_2 . The two solid phases, ZrO_2 and SiO_2 , co-exist represented by the horizontal tie lines between $1687^\circ C$ and $1673^\circ C$ and SiO_2 melting temperature is $1723^\circ C$. Eutectic reaction occurs on the SiO_2 -rich region at $1687^\circ C$, but SiO_2 is not soluble in ZrO_2 . The melting temperature of ZrO_2 is $2680^\circ C$ and exists as monoclinic $-ZrO_2$ at room temperature with transformation to tetragonal $-ZrO_2$ at $1205^\circ C$ and the tetragonal $-ZrO_2$ to cubic fluorite $-ZrO_2$ transformation at $2370^\circ C$. There is a 9% volume increase when tetragonal $-ZrO_2$ transforms to monoclinic $-ZrO_2$. The liquidus line exists over the entire region with a miscibility gap between $2250^\circ C$ and $2430^\circ C$ indicated by $L1 + L2$.

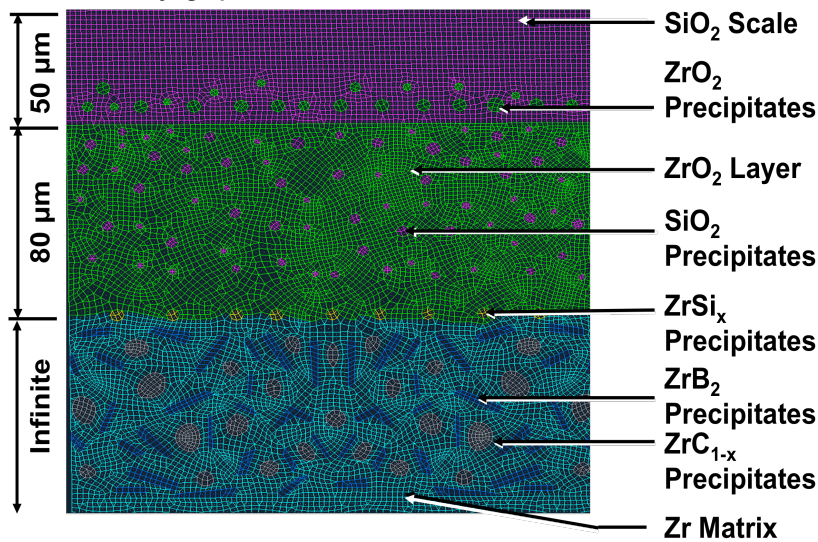


Figure 2.6: FEA model of the ZrB_2 - ZrC - Zr Composite with Oxide Scales [Petla-2010].

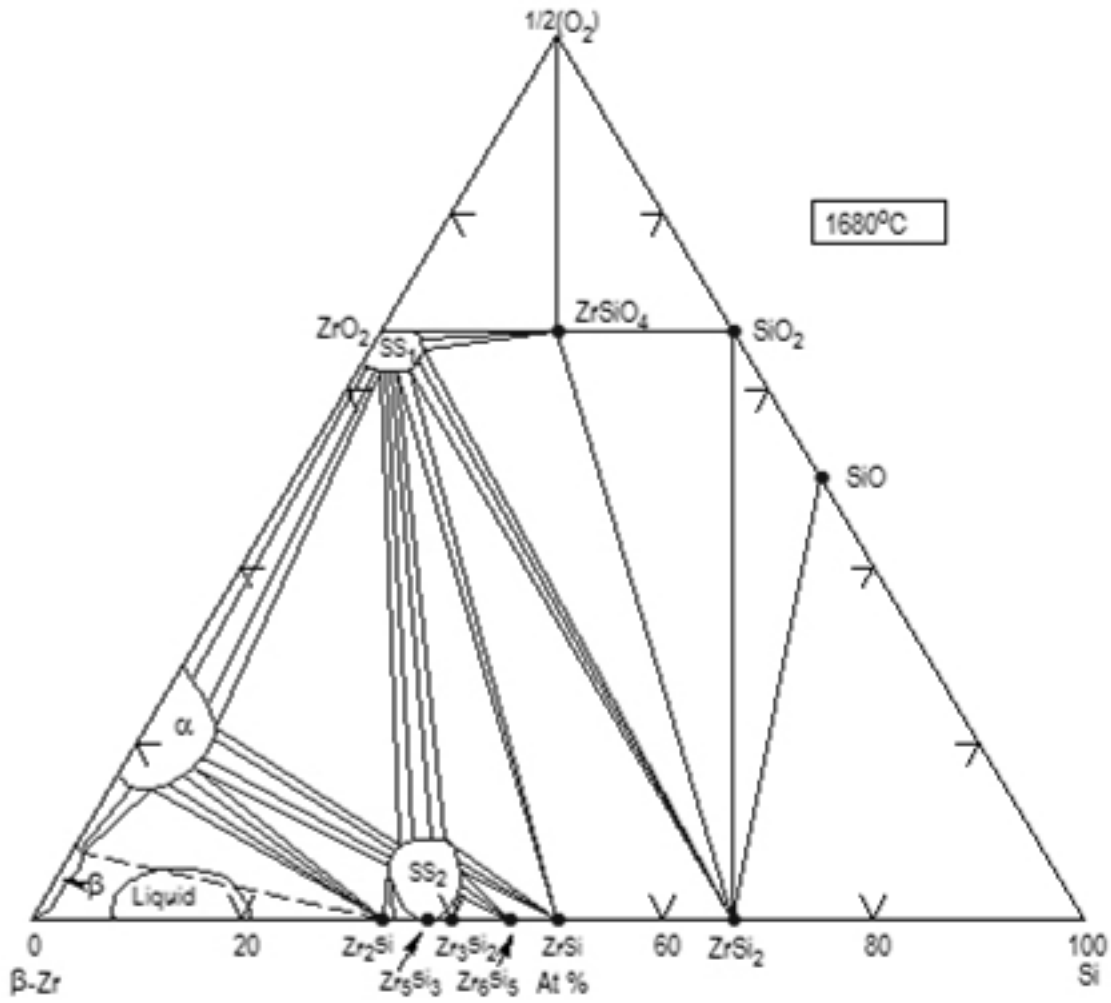


Figure 2.7: Zr-Si-O Ternary Phase Diagram at 1680°C [Sorrell-1986].

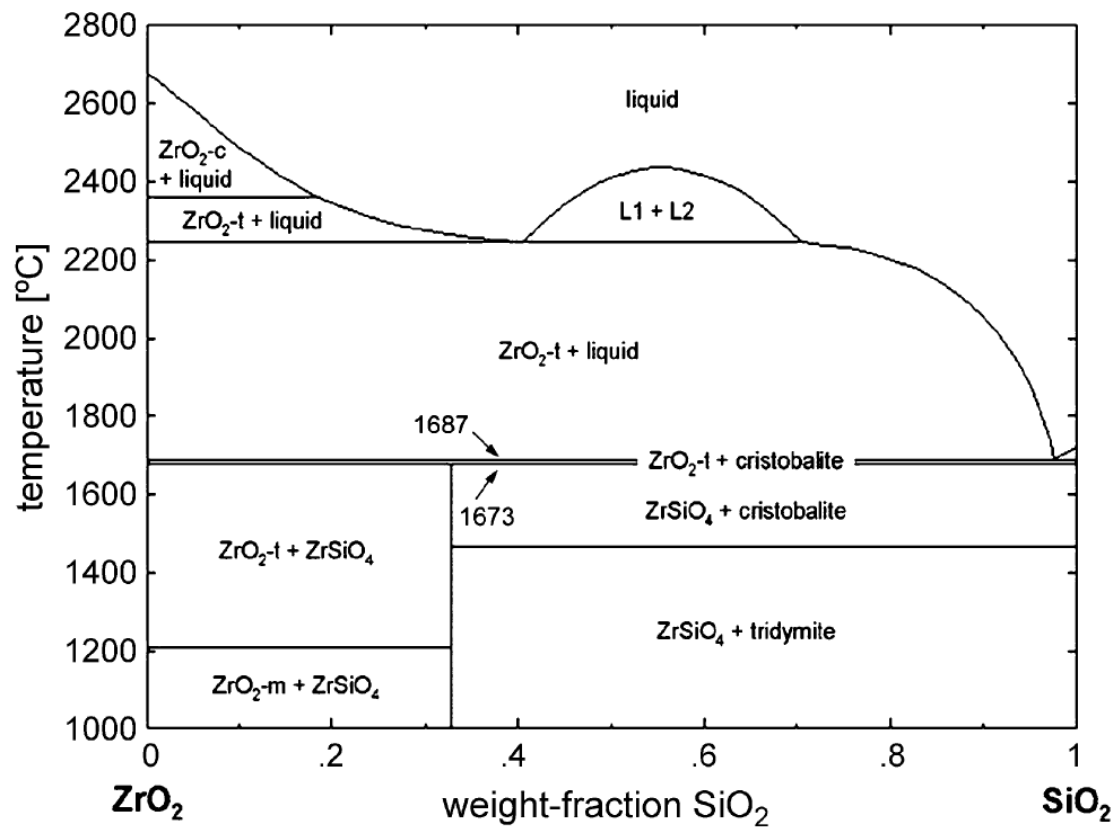


Figure 2.8: ZrO₂-SiO₂ Pseudo-Binary Phase Diagram [Kaiser-2008].

Chapter 3: RESEARCH METHODOLOGY

3.1: Sample Preparation

B_4C powder (99+%, < 10 micron) and $ZrSi_2$ (99.5%, -325 mesh) supplied by Alfa Aesar was packed into a graphite crucible (0.5" OD, 1mm thick and 0.6" length) acquired from LECO. Zr slugs (99.5%, 3.175 mm diameter and 3.175 mm length), also obtained from Alfa Aesar, and was then placed on top of the $ZrSi_2$ powder. Graphite covers were used at the top of the graphite crucibles to push back the levitating Zr-Si melt. Two different compositions of $ZrSi_2$ were used, 0.57 g and 0.8 g, with the weights of B_4C (0.25 g) and Zr (1.5 g) kept constant. The 0.57 g sample corresponds to Zr-12wt%Si and 0.8 g sample corresponds to Zr-16wt%Si on the Zr-Si phase diagram. The sample setup is shown in figure 3.1.

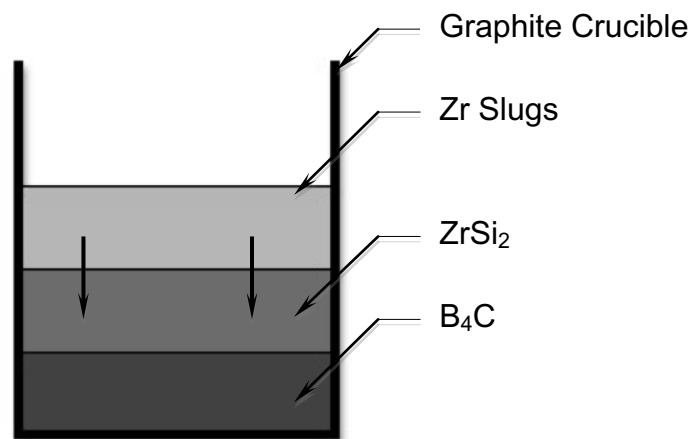


Figure 3.1: Sample Setup.

The samples were then placed in a graphite enclosure (Figures 3.3 and 3.4) machined from a graphite rod (2" diameter \times 17" length) acquired from American Graphite Corporation. Figure 3.2 shows the graphite enclosure insulated by zirconia

grog (-8/+20 mesh) sourced from Zircoa. A zirconia crucible sufficiently shielded the graphite enclosure from the high magnetic fields generated by the induction furnace. GM Associates supplied the quartz reaction tube and CoorsTek, Inc supplied the zirconia crucible stabilized with Y_2O_3 (35 mm diameter \times 64 mm length). Pure aluminum wire (99.999%, 0.81mm diameter) procured from Alfa Aesar was rolled around the bottom part of the graphite enclosure, which oxidized to form a seal, thereby creating an inert atmosphere inside the graphite crucible. Titanium slugs and aluminum slugs were placed in the Al-Ti melt pit, as shown in figure 3.4, was used for the purpose of removing any residual oxygen left inside the graphite enclosure. The titanium slugs (99.5%, 3.175 mm diameter and 3.175 mm length) and aluminum slugs (99.5%, 3.175 mm diameter and 3.175 mm length) were sourced from Alfa Aesar.

3.2: Experimental Procedure

The $ZrB_2-ZrC-Zr_xSi_y$ composite was processed in an induction furnace with operating frequency of 4.5 MHz with temperature controlled by an Ircon Maxline CPU™ infrared pyrometer sighting on the graphite enclosure. The induction furnace was acquired from Thermal Technology Inc. The set temperature was little more than the melting temperature of Zr at 1860 °C, but due to the exothermic reactions, temperatures inside the graphite enclosure will be in the region of 2300 °C – 2400°C [Johnson-1991]. Deoxidized helium gas was passed through the entire setup, which is shown in figure 3.5. Helium gas was preferred over argon gas to avoid plasma formation. The purification of helium was achieved in 3 steps. First, helium gas was passed through a column of magnesium perchlorate to remove moisture. Two subsequent steps of passing the He gas through tubes containing titanium sponge, obtained from Alfa Aesar,

column of magnesium perchlorate to remove moisture. Two subsequent steps of passing the He gas through tubes containing titanium sponge, obtained from Alfa Aesar, deoxidized the gas. The first tube with titanium sponge was maintained at 700°C and the second tube was maintained at 800°C bringing down the oxygen potential of helium gas to 10^{-60} atm before entering the reaction tube setup. The helium gas was vented out into a dibutylphthalate bubbler. Diagrams of the reaction tube, reaction tube cap, cooling jacket, lower bottom reaction tube cap, and cooling jacket cap are shown from figures 3.6 – 3.10.

The experiments were successfully run by holding the induction furnace at 1860°C for 60, 120, 180, and 240 minutes with the last reacting time giving sufficient time for the entire melt to equilibrate. The temperature ramp rate was 30 °C/minute from room temperature to 1000 °C and 8 °C/minute from 1000 °C to 1860 °C, which is the set temperature. At the end of the experiment, rapid cooling was maintained to freeze the microstructure achieved at higher temperatures. Temperature calibration was achieved by placing platinum wire on the graphite enclosure, which could be seen through the sighting tube of the pyrometer. When the platinum wire melted at its melting temperature of 1773 °C, the temperature was increased on the controller by 87 °C, the difference between the set temperature of 1860 °C and platinum melting temperature of 1773°C.

3.3: Microstructure Characterization

The processed samples were cut along its length using a Struers – Accutom 2

table saw equipped with a diamond cut off wheel. The cross sections were then mounted on epoxy resin supplied by Pace Technologies and prepared by grinding with 120, 240, 400, 600, 800, and 1000 grit paper and finished by polishing with 1 μ m diamond paste. The polished samples were rinsed with water and methanol before drying them with a blower. The microstructures of the cross sectioned samples were analyzed with scanning electron microscope (Hitachi), optical microscope (Reichert) and X-ray diffractometer (Bruker). The X-ray diffractometer was operating with an accelerating voltage of 40 kV and a beam current of 40 mA for an angle 2θ of 10 $^{\circ}$ -70 $^{\circ}$.

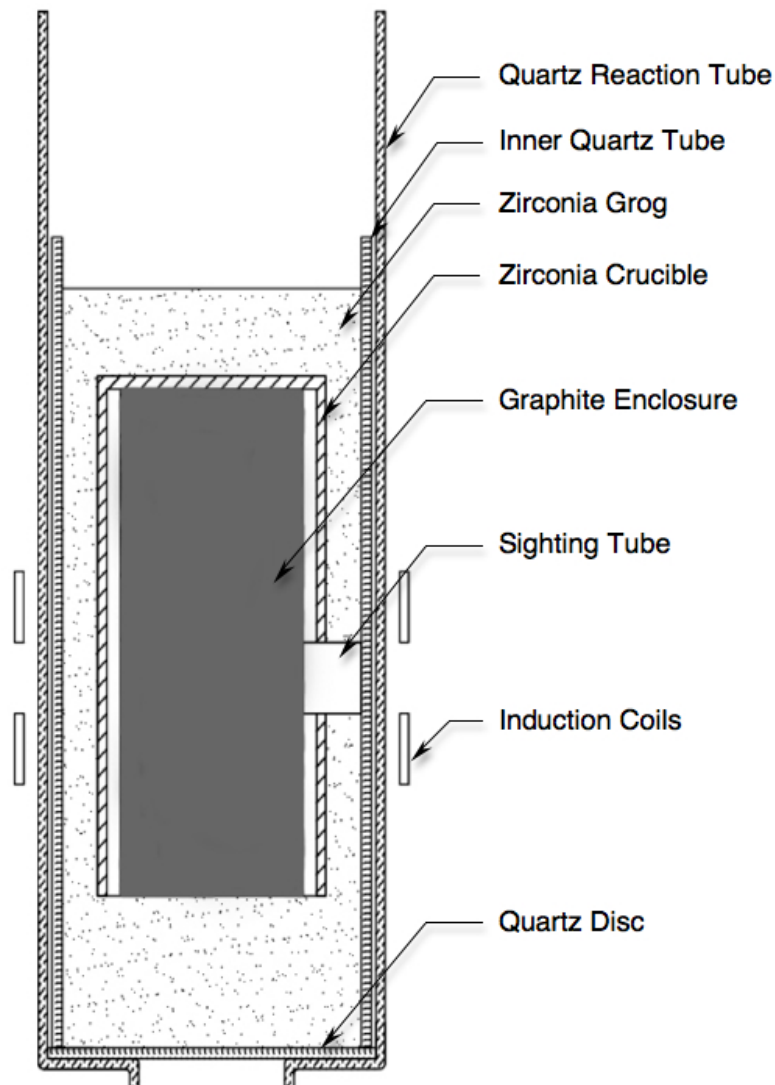


Figure 3.2: Graphite Enclosure Setup.

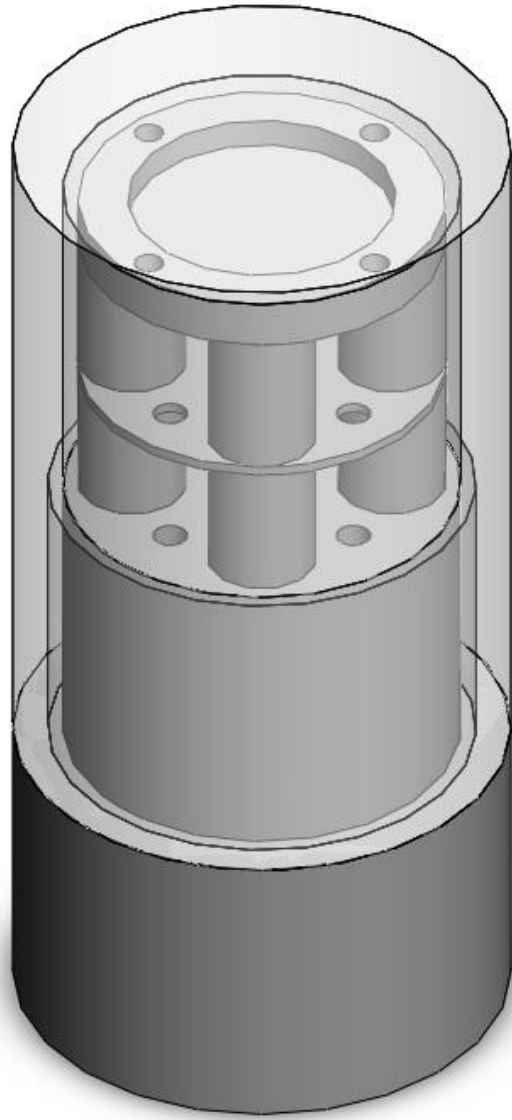


Figure 3.3: Graphite Enclosure with Graphite Crucible Sample.

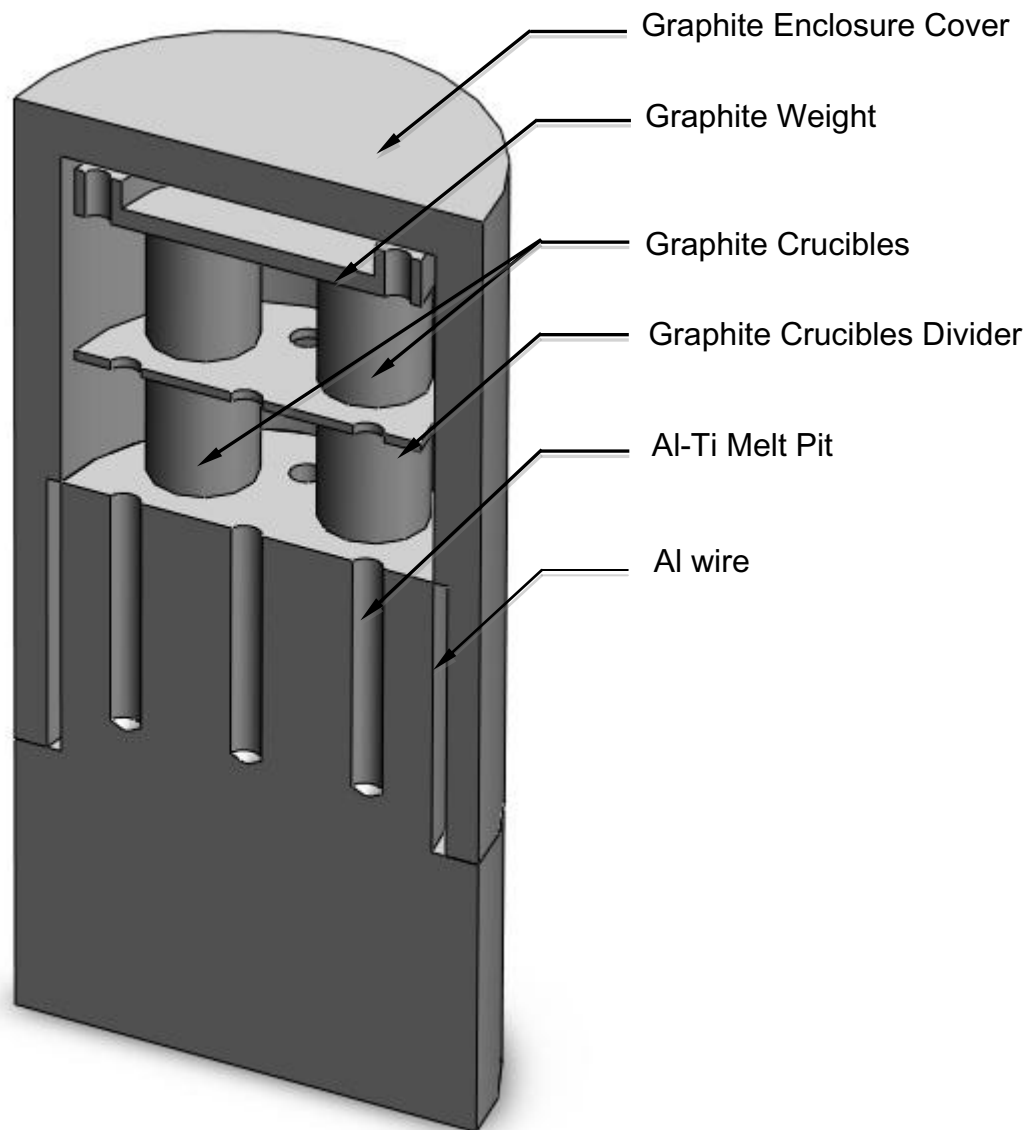


Figure 3.4: Cross-section of the Graphite Enclosure.

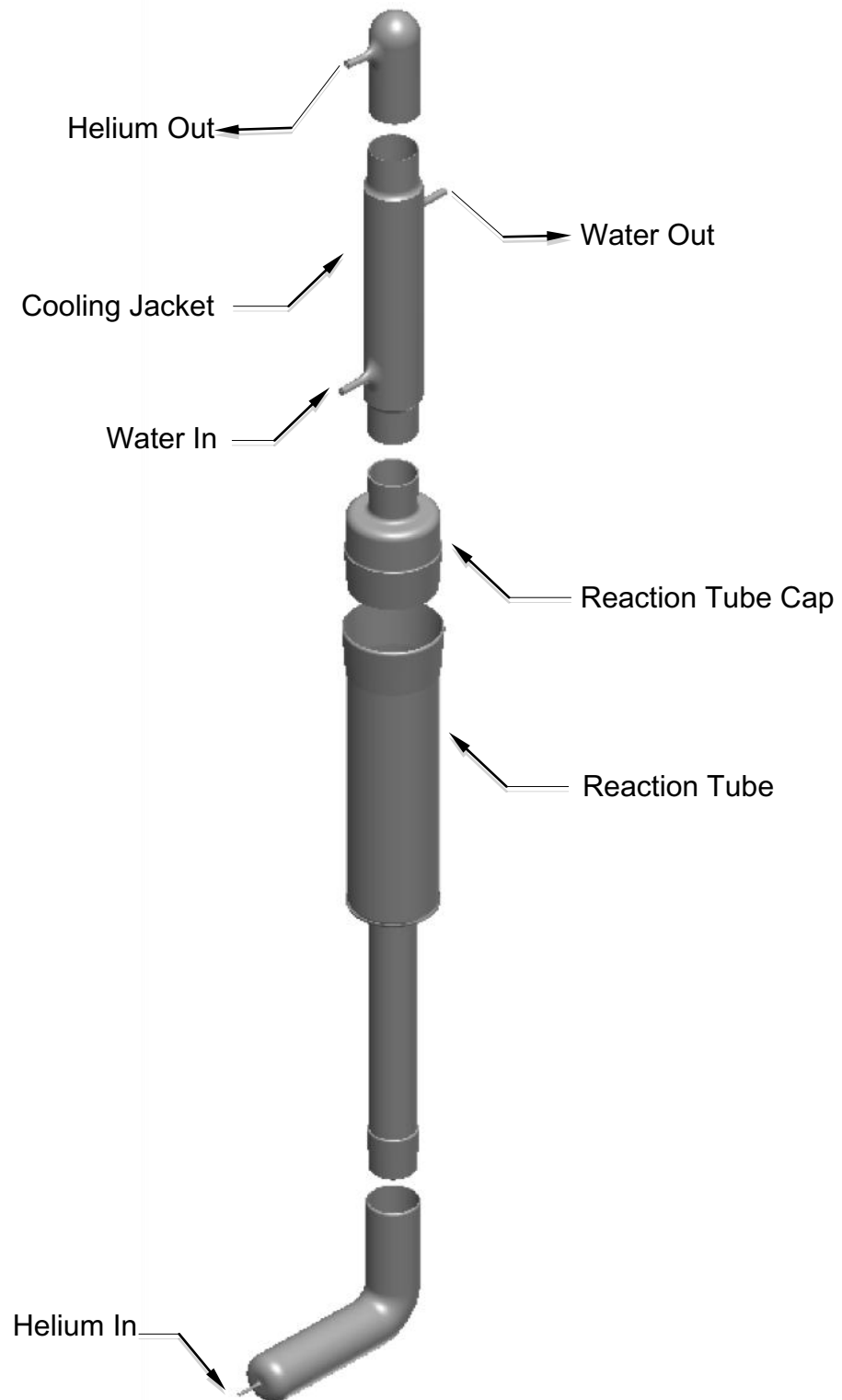


Figure 3.5: Reaction Tube Setup.

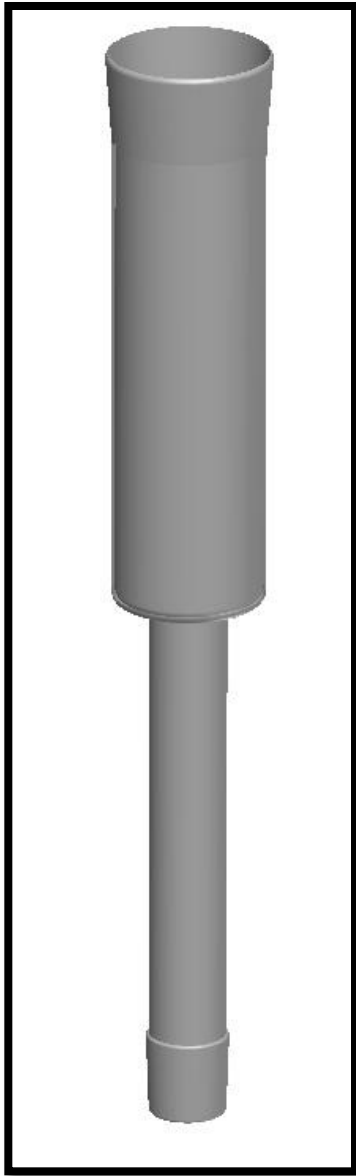


Figure 3.8: Quartz Reaction Tube.

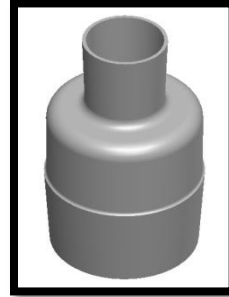


Figure 3.6: Reaction Tube Cap.

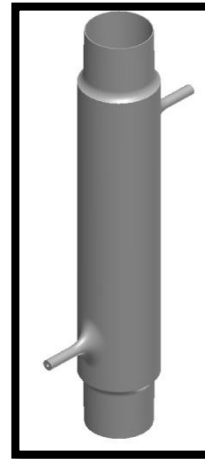


Figure 3.7: Cooling Jacket.

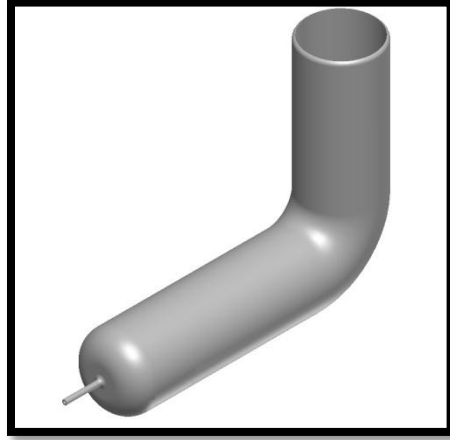


Figure 3.9: Bottom Reaction Tube Cap.

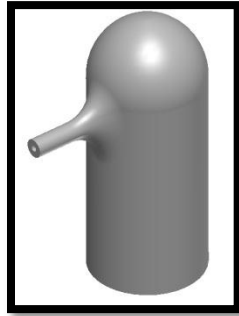


Figure 3.10: Cooling Jacket Cap.

Chapter 4: RESULTS

In this chapter, X-ray diffraction patterns and micrographs of the processed composites are described. The starting compositions of the samples were Zr-12wt%Si and Zr-16wt%Si with B₄C constant at 0.25 g and they were heated at the set temperature of 1860 °C for 60, 120, 180, and 240 minutes. The formation of pellet-like composites was not possible due to the zirconium levitation caused by the electromagnetic field of the induction furnace. The electromagnetic field brought about mixing of the melt at different places inside the graphite crucible leaving behind a highly heterogeneous microstructure. Description of accurate interfacial reactions, which occurred during the process, is not feasible due to the melt solidifying at different places on the graphite crucible. All samples observed showed varying porosity and grain size with greater porosity for shorter duration of reaction time. The increased porosity for shorter reaction times is due to the incomplete reactions between the free B₄C and the Zr-Si melt. An example of a levitating composite is shown in figure 4.1. Visual inspection and XRD analysis of the cross-sectioned samples showed no oxides scales demonstrating the removal of the residual oxygen inside the graphite enclosure and proper sealing by the aluminum wire and the Al-Ti melt.

4.1: X-Ray Diffraction

X-ray diffraction patterns for Zr-12 wt% Si samples and Zr-16 wt% Si samples heated at 1860°C for 60, 120, 180, and 240 minutes are shown in figures 4.2 to 4.9. The analysis of the diffracting spectra identified ZrB₂ and ZrC in all four groups. A single-phase silicide, ZrSi is shown to exist in both compositions of the samples processed at

1860°C for all the four groups. In 120 minutes group, almost similar x-ray diffraction patterns were observed compared to samples annealed at 1860 °C for 60 minutes, with the exception of the appearance of another silicide, Zr_5Si_4 (tetragonal crystal structure). Almost identical patterns are acquired for samples allowed to react for 180 minutes and 240 minutes. One exception is the Zr -12 wt% Si sample reacted for 240 minutes, in which peaks matching silicide, Zr_2Si , was found (figure 4.8).

4.2: Microstructures

The SEM and optical micrograph for 60 minutes as shown in figure 4.10 and 4.11 points to the ZrB_2 precipitates (hexagonal crystal structure) and ZrC precipitates (face-centered cubic crystal structure) dispersed in a Zr-Si melt. The unreacted B_4C is shown on the right in the optical micrograph. ZrB_2 , ZrC and Zr_xSi_y precipitates surrounded by the unreacted B_4C are shown in figure 4.11. B_4C was observed in the samples reacted for 120 minutes too (figure 4.13), indicating incomplete reactions. But, micrographs for samples reacted for 180 and 240 minutes (figures 4.15 to 4.17) demonstrates complete reaction between B_4C and Zr-Si melt forming a continuous microstructure with ZrB_2 , the most dominant phase.

4.3: Results Summary

ZrB_2 was the main phase in the matrix after reaction. $ZrSi$ was the only silicide identified by XRD in all 4 groups. Zr_5Si_4 was detected in 3 groups excluding the 60 minutes run. Zr_2Si was spotted only in the Zr -16 wt% Si sample heated at the set temperature for 240 minutes. Other silicides like Zr_5Si_3 , Zr_3Si , and $ZrSi_2$ were not observed on the x-ray spectrum s. Micrographs for the 4 groups showed formation of ZrB_2 -ZrC composite in a solidified Zr-Si melt. Large amounts of free B_4C were observed

in the shorter runs of 60 minutes and 120 minutes and considerable porosity were observed in all the samples. To conclude, ZrB_2 and ZrC precipitates within a metal matrix of a Zr-Si alloy were successfully developed in both sets of compositions heated at 1860°C for 60, 120, 180, and 240 minutes

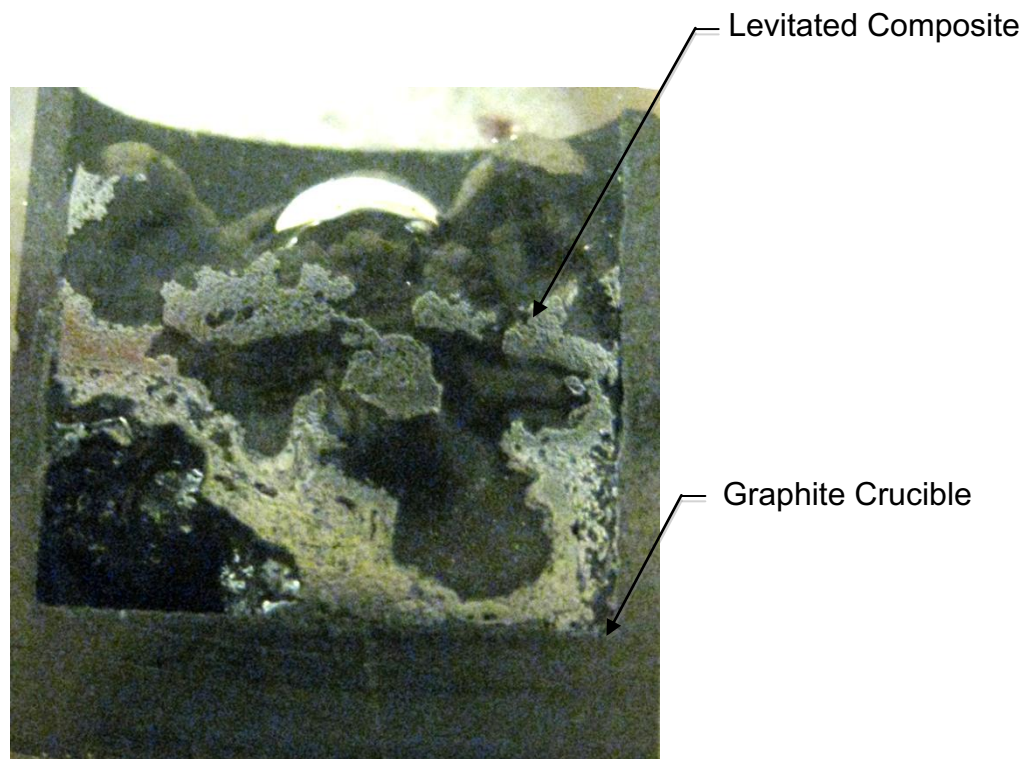


Figure 4.1: Cross-section of a processed sample showing the effect of the levitation caused by the magnetic field of the induction furnace.

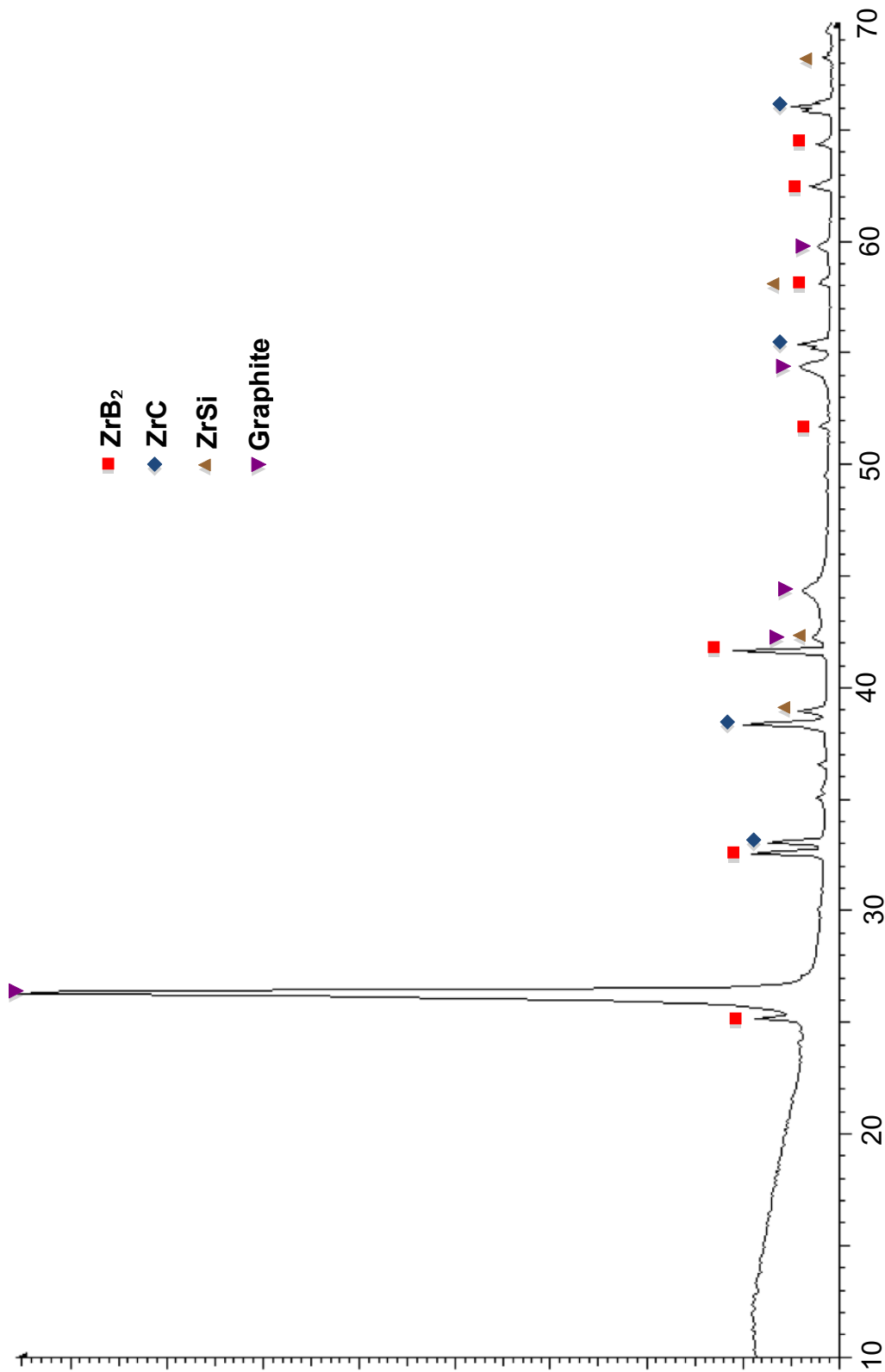
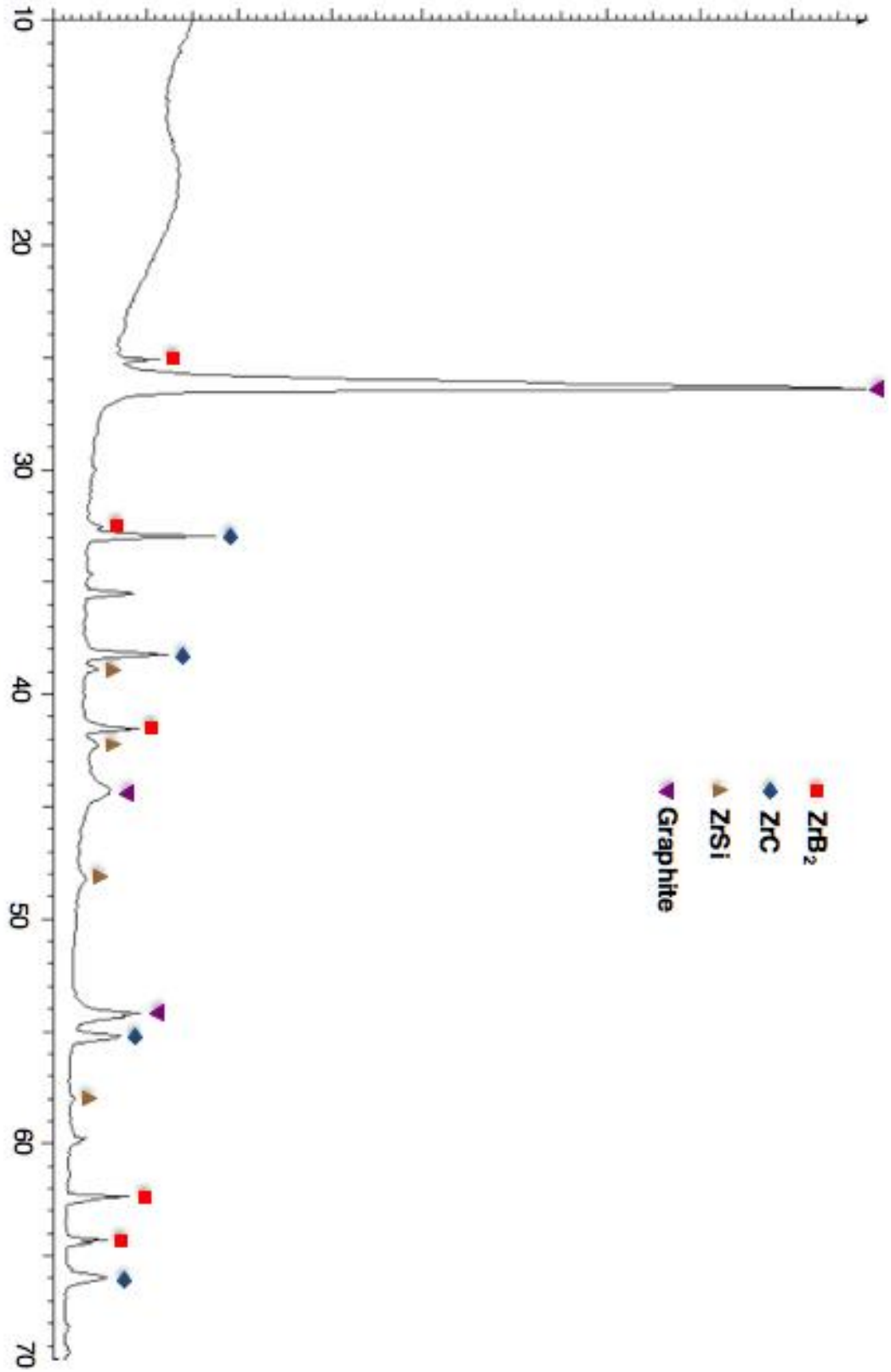


Figure 4.2: XRD diagram for Zr-12wt%Si held at 1860°C for 60 minutes.

Figure 4.3: XRD diagram for Zr-16wt%Si held at 1860°C for 60 minutes.



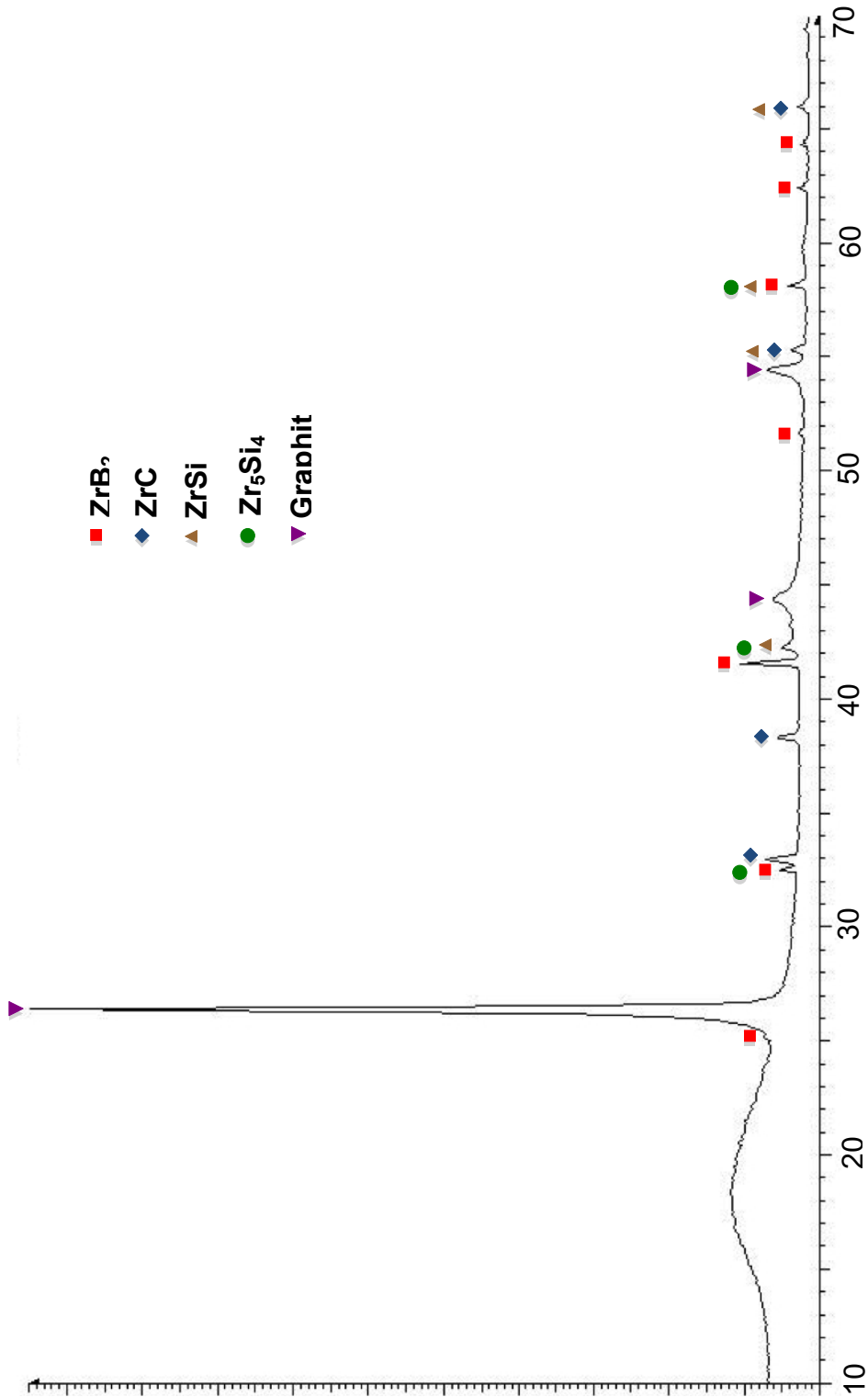


Figure 4.4: XRD diagram for Zr-12wt%Si held at 1860°C for 120 minutes.

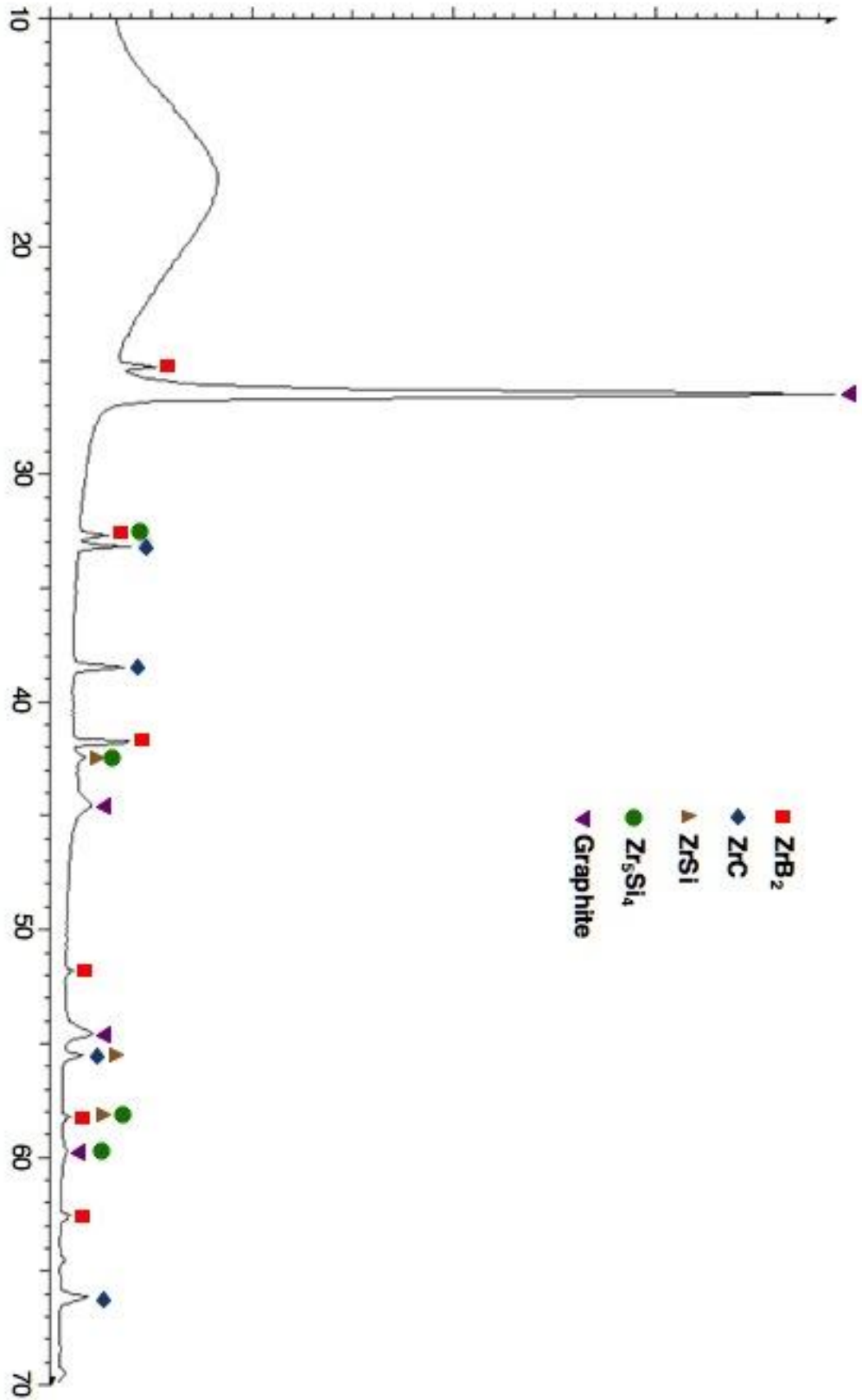


Figure 4.5: XRD diagram for Zr-16wt%Si held at 1860°C for 120 minutes.

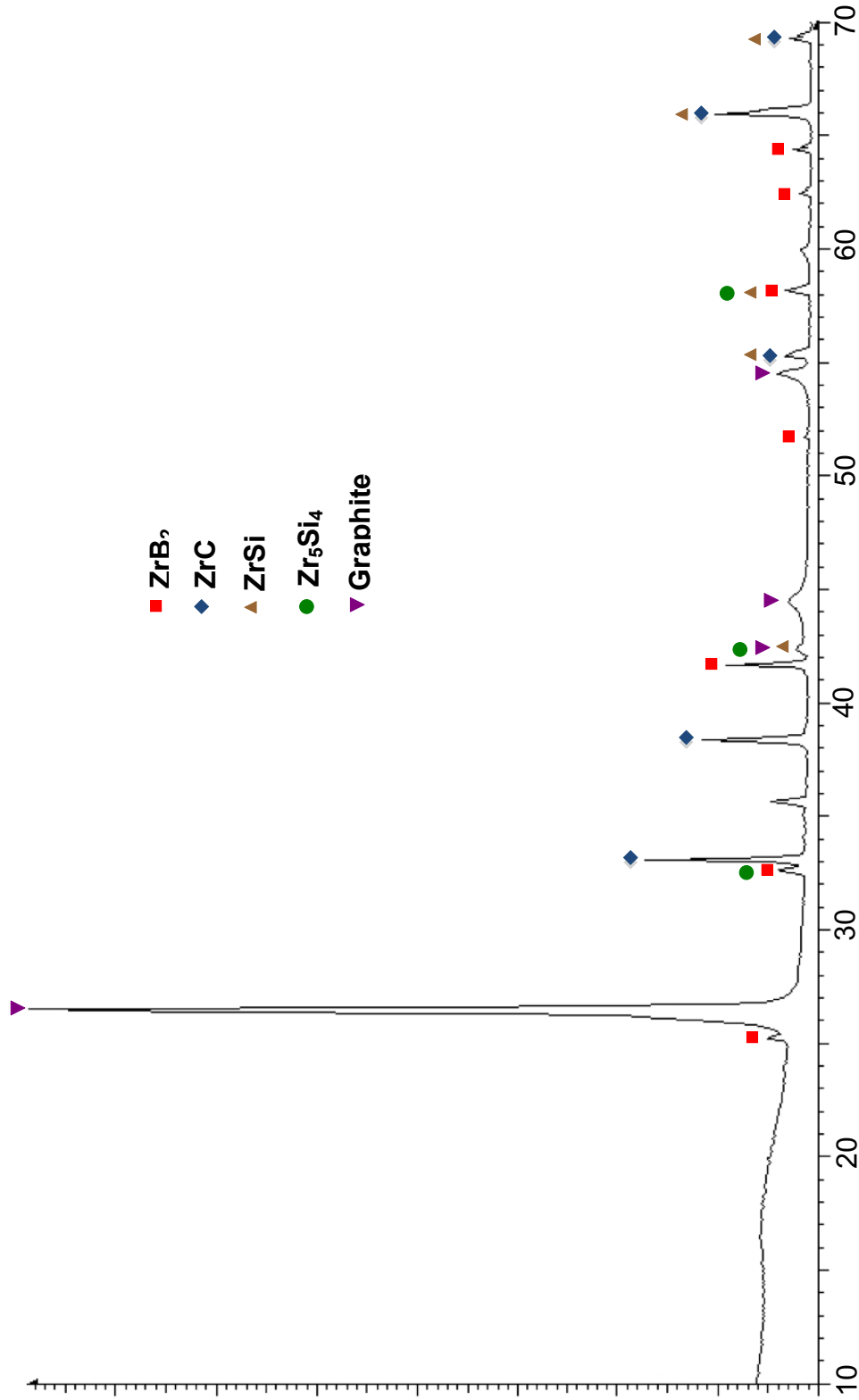


Figure 4.6: XRD diagram for Zr-12wt%Si held at 1860°C for 180 minutes.

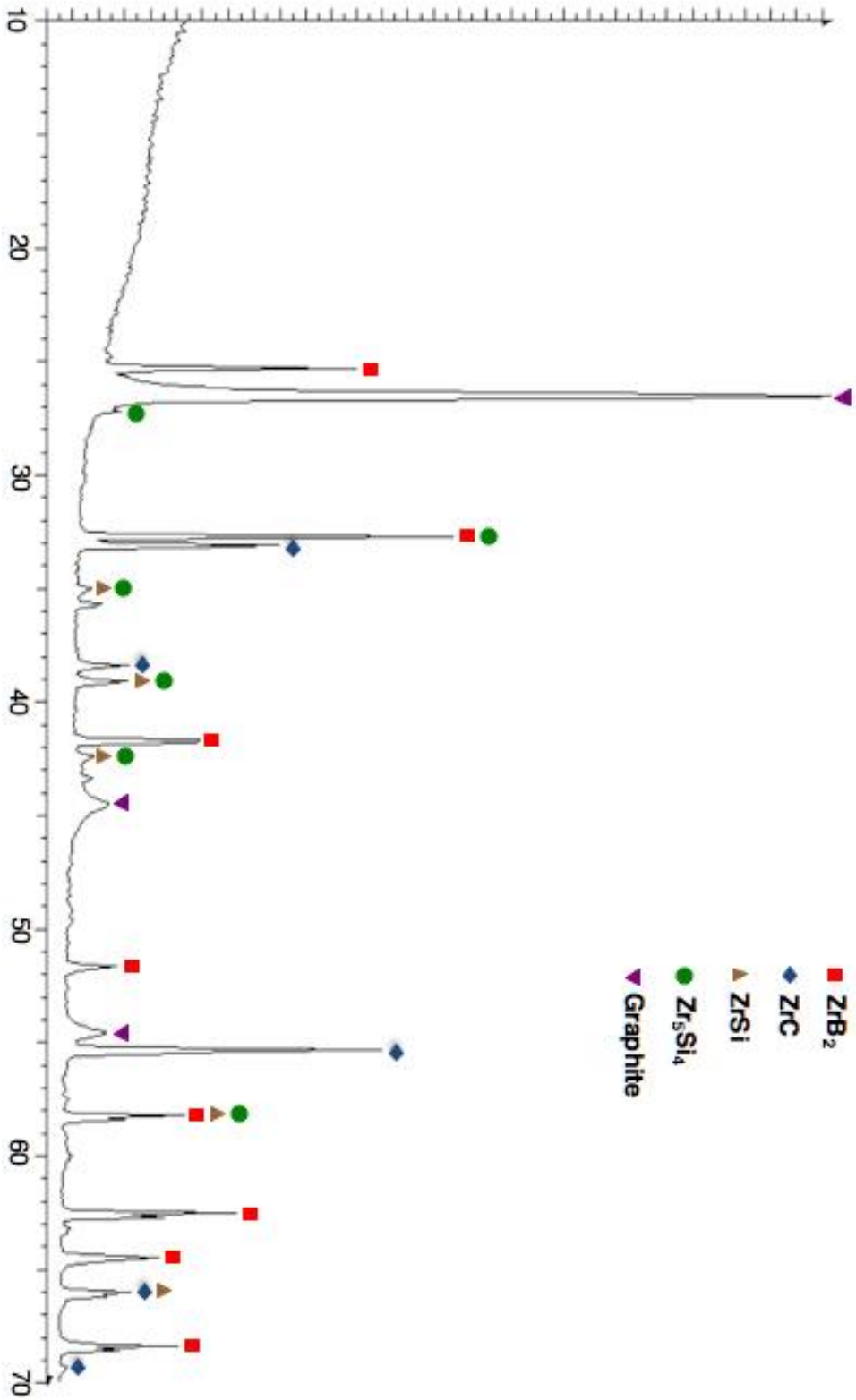


Figure 4.7: XRD diagram for Zr-16wt%Si held at 1860°C for 180 minutes.

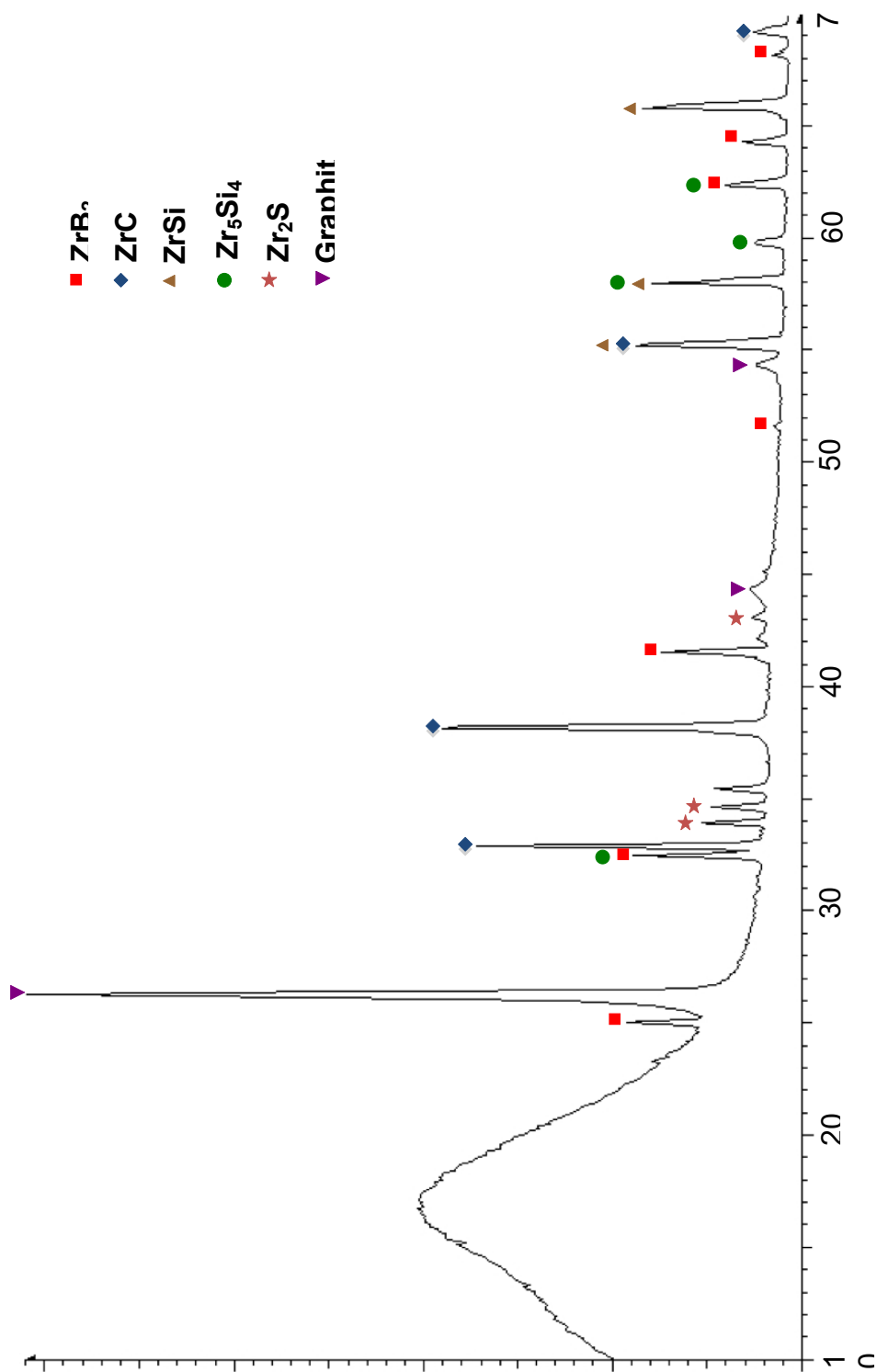


Figure 4.8: XRD diagram for Zr-12wt%Si held at 1860 °C for 240 minutes.

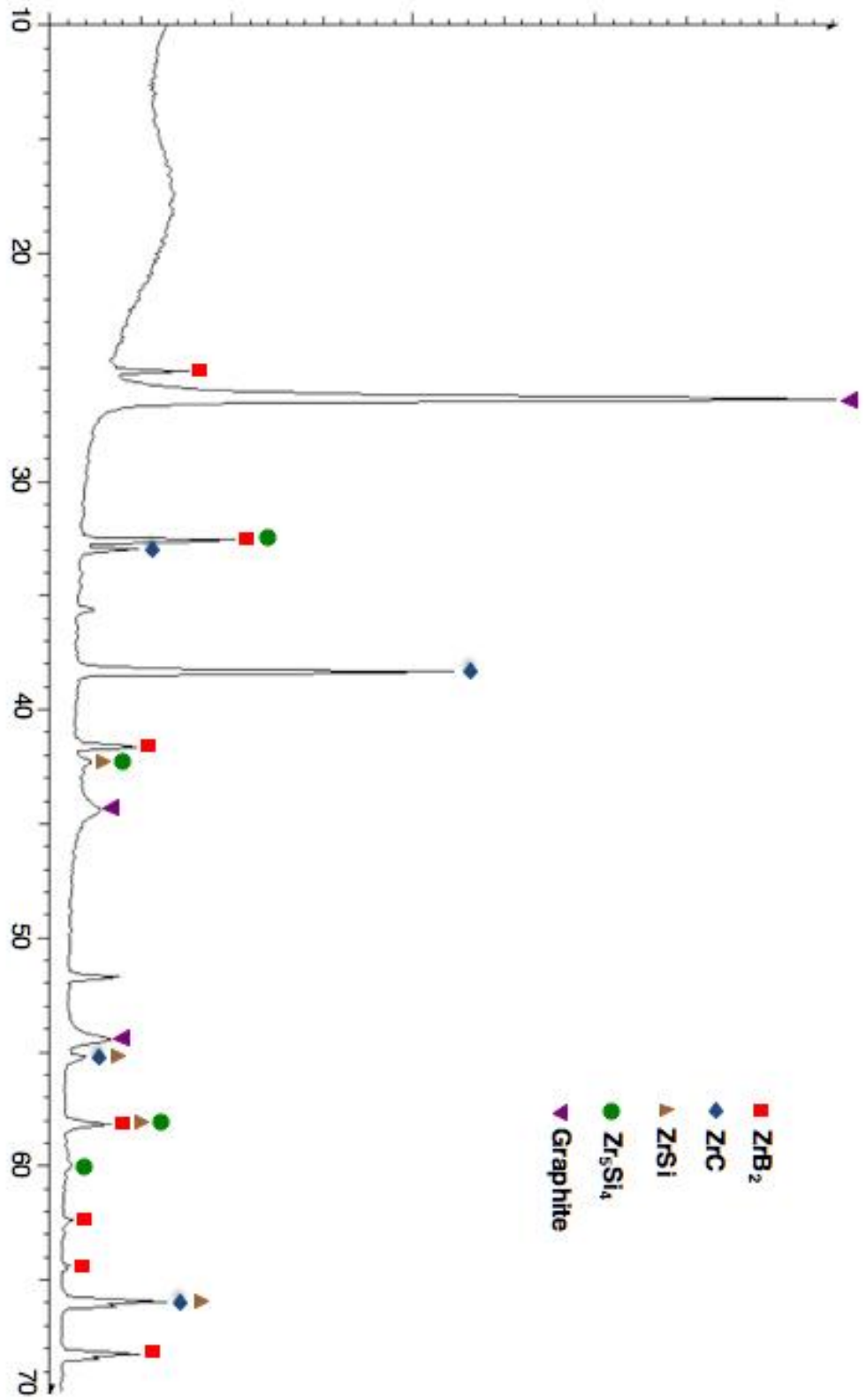


Figure 4.9: XRD diagram for Zr-16wt%Si held at 1860°C for 240 minutes.

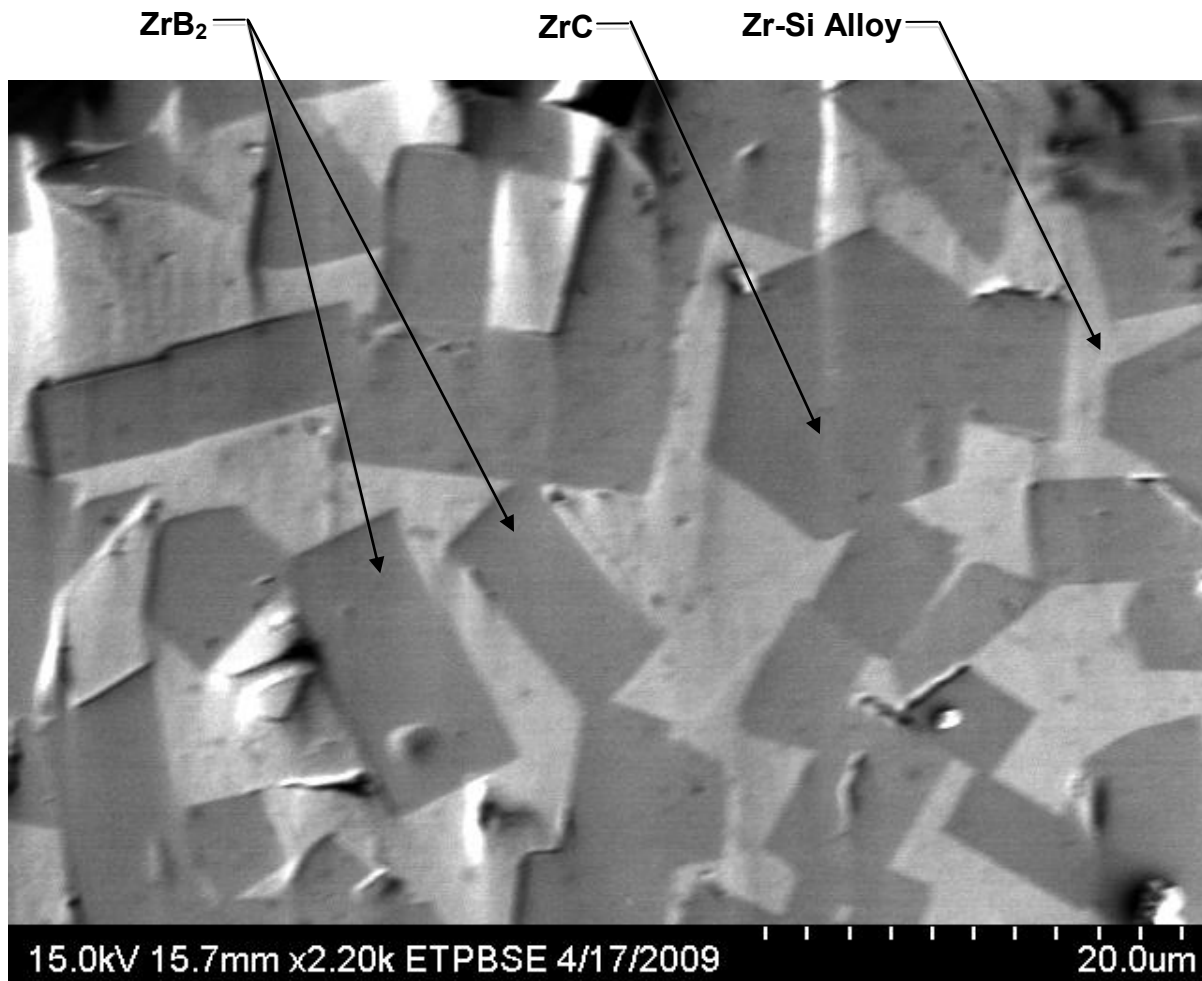


Figure 4.10: SEM Micrograph of ZrB₂-ZrC precipitates surrounded by solidified Zr-Si melt and the unreacted B₄C in sample held at 1860°C for 60 minutes.

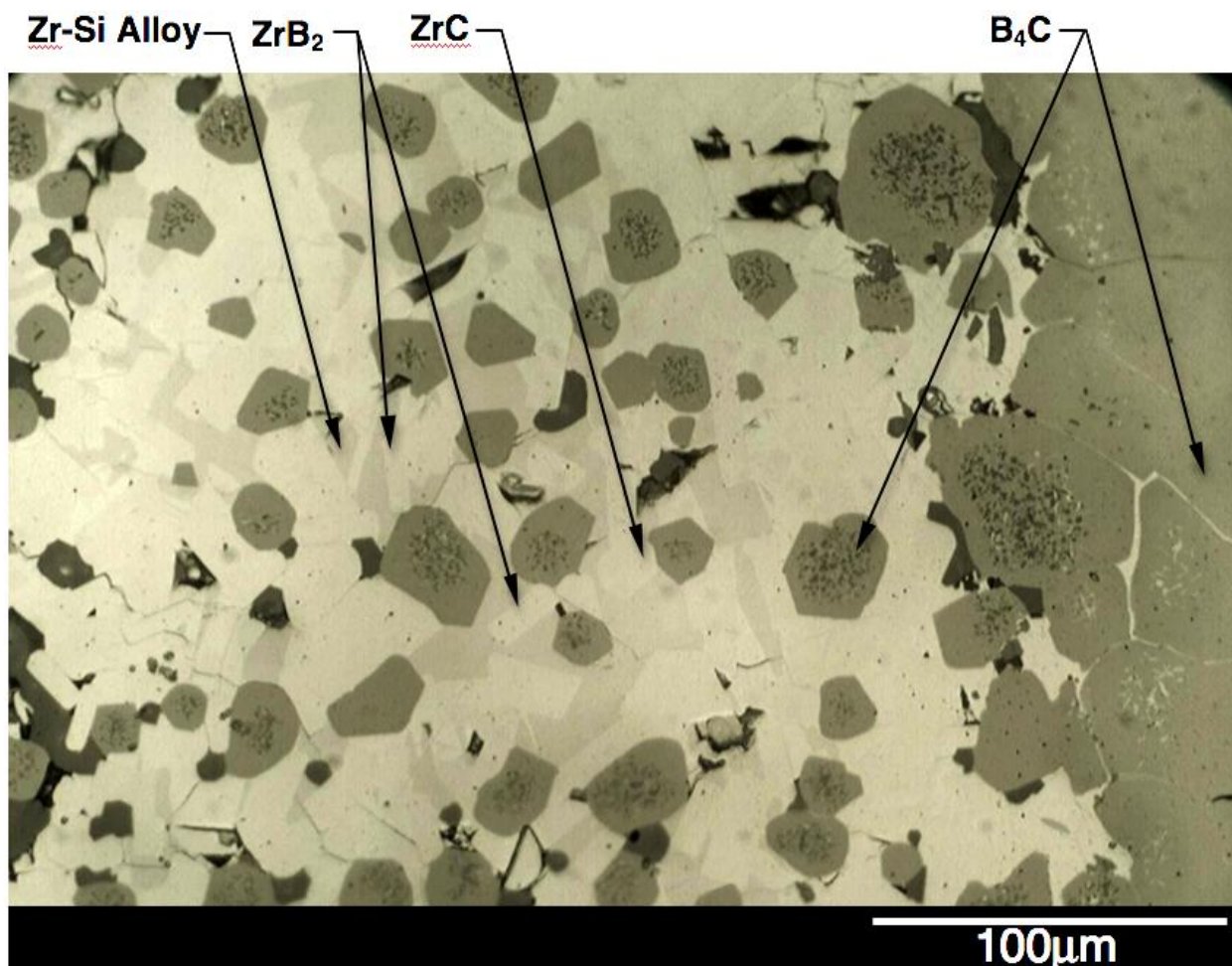


Figure 4.11: Micrograph of ZrB₂-ZrC precipitates surrounded by solidified Zr-Si melt and the unreacted B₄C in sample held at 1860°C for 60 minutes.

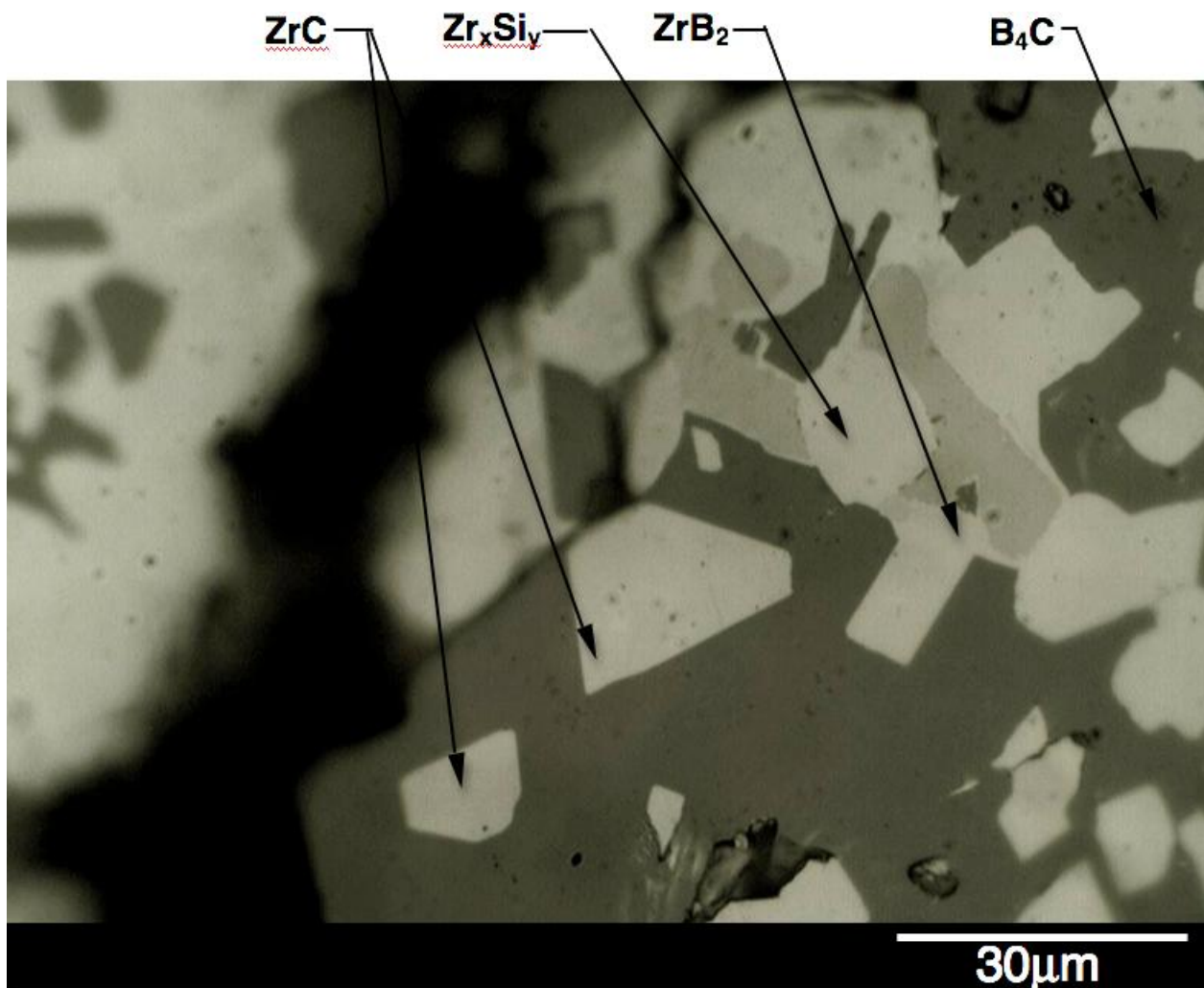


Figure 4.12: Micrograph with a closer look at the unreacted B_4C and ZrB_2 - ZrC - Zr_xSi_y precipitates in sample held at $1860^\circ C$ for 60 minutes.

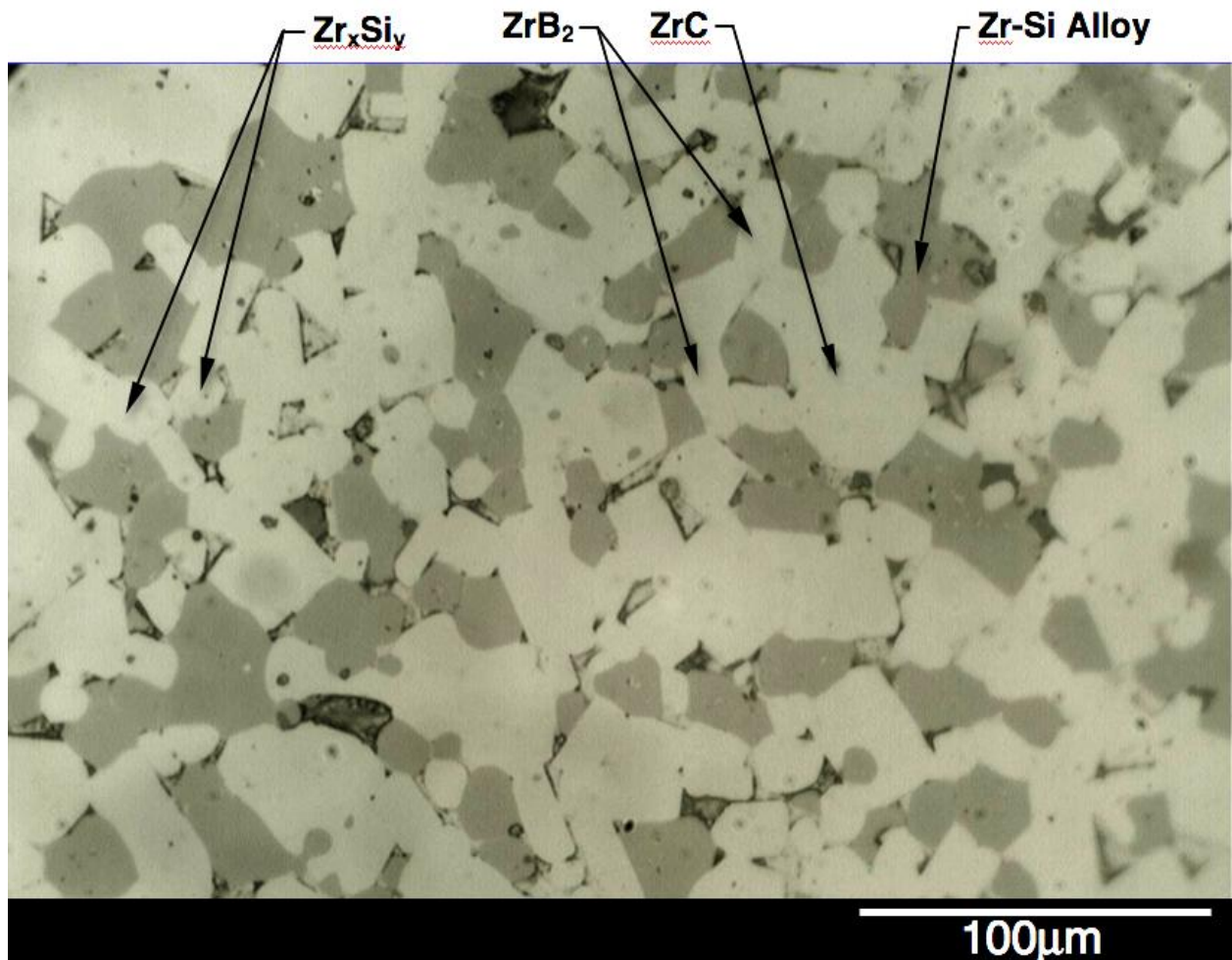


Figure 4.13: Micrograph of ZrB_2 - ZrC - Zr_xSi_y precipitates encased within solidified Zr-Si melt in a sample held at $1860^\circ C$ for 120 minutes.

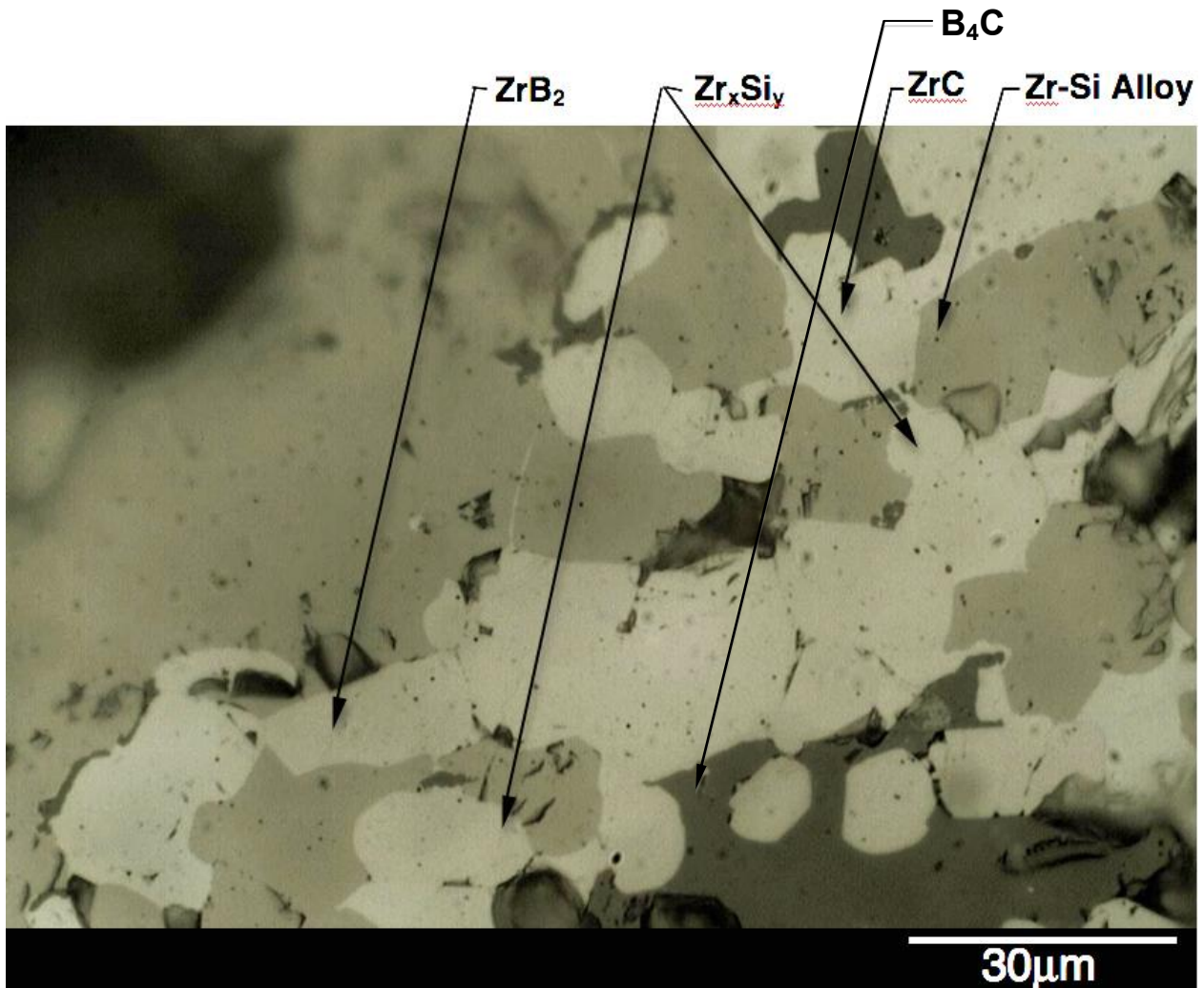


Figure 4.14: Micrograph with a closer look at the unreacted B_4C and ZrB_2 - ZrC - Zr_xSi_y precipitates in sample held at $1860^\circ C$ for 120 minutes.

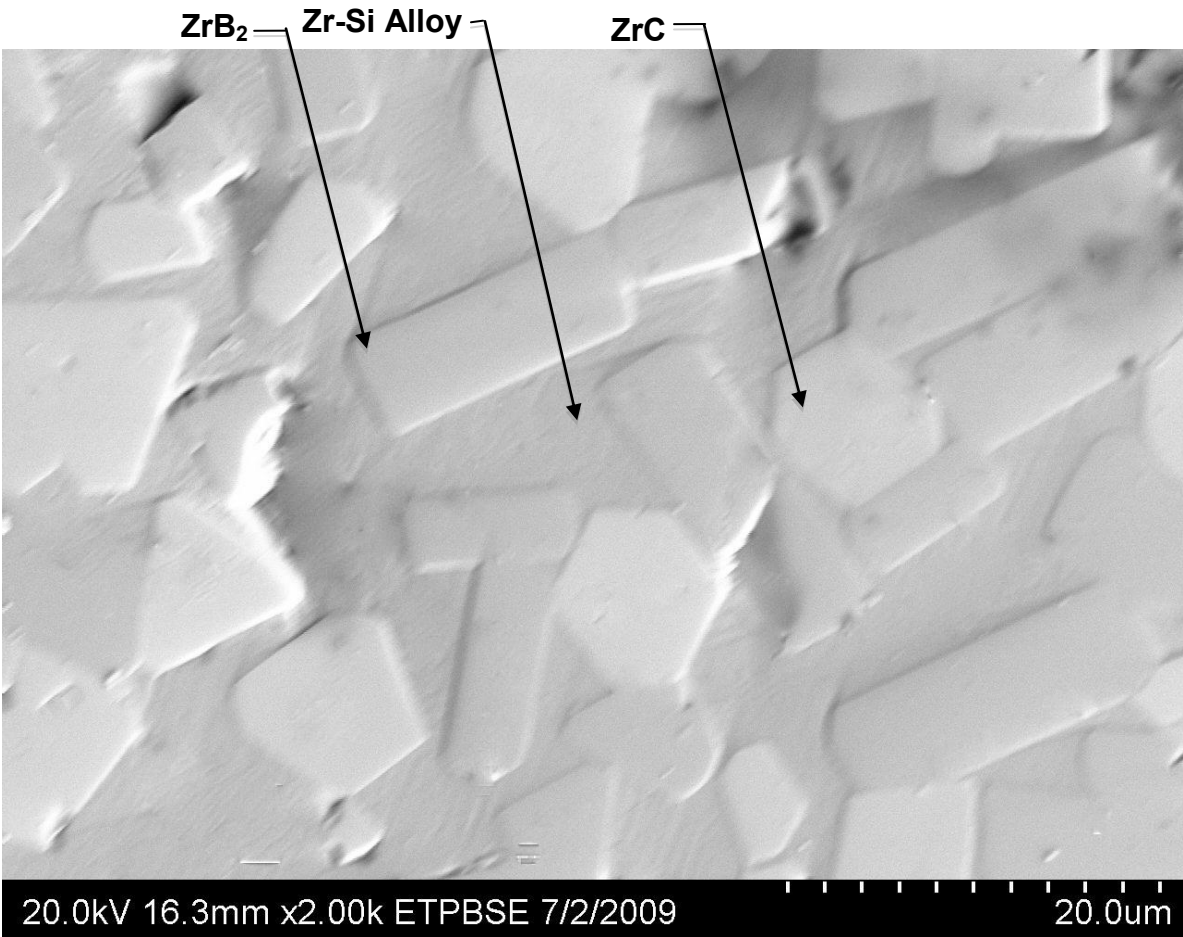


Figure 4.15: Micrograph of ZrB₂-ZrC precipitates encased within solidified Zr-Si melt in a sample held at 1860°C for 180 minutes.

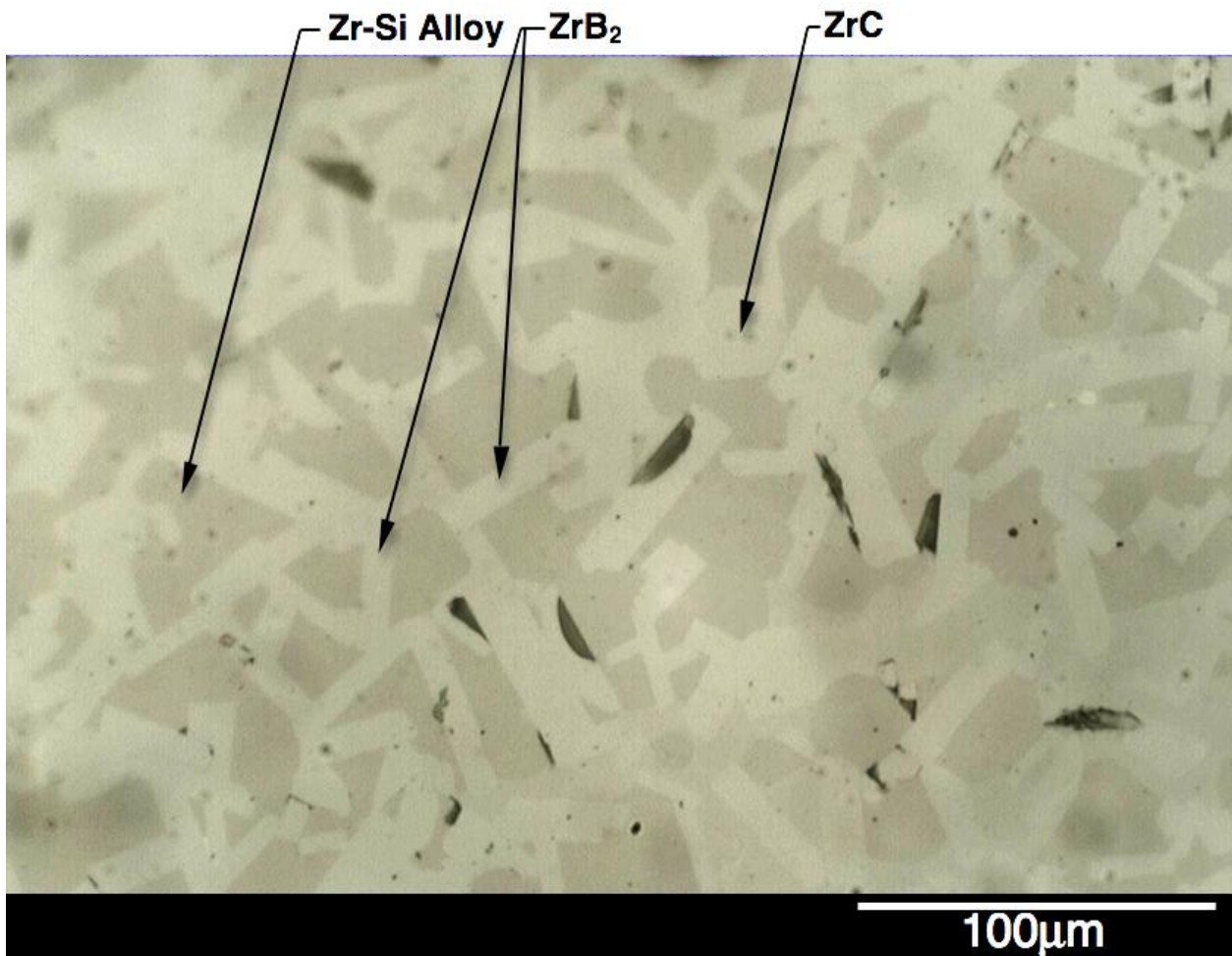


Figure 4.16: Micrograph of ZrB₂-ZrC precipitates in a completely reacted sample held at 1860°C for 180 minutes.

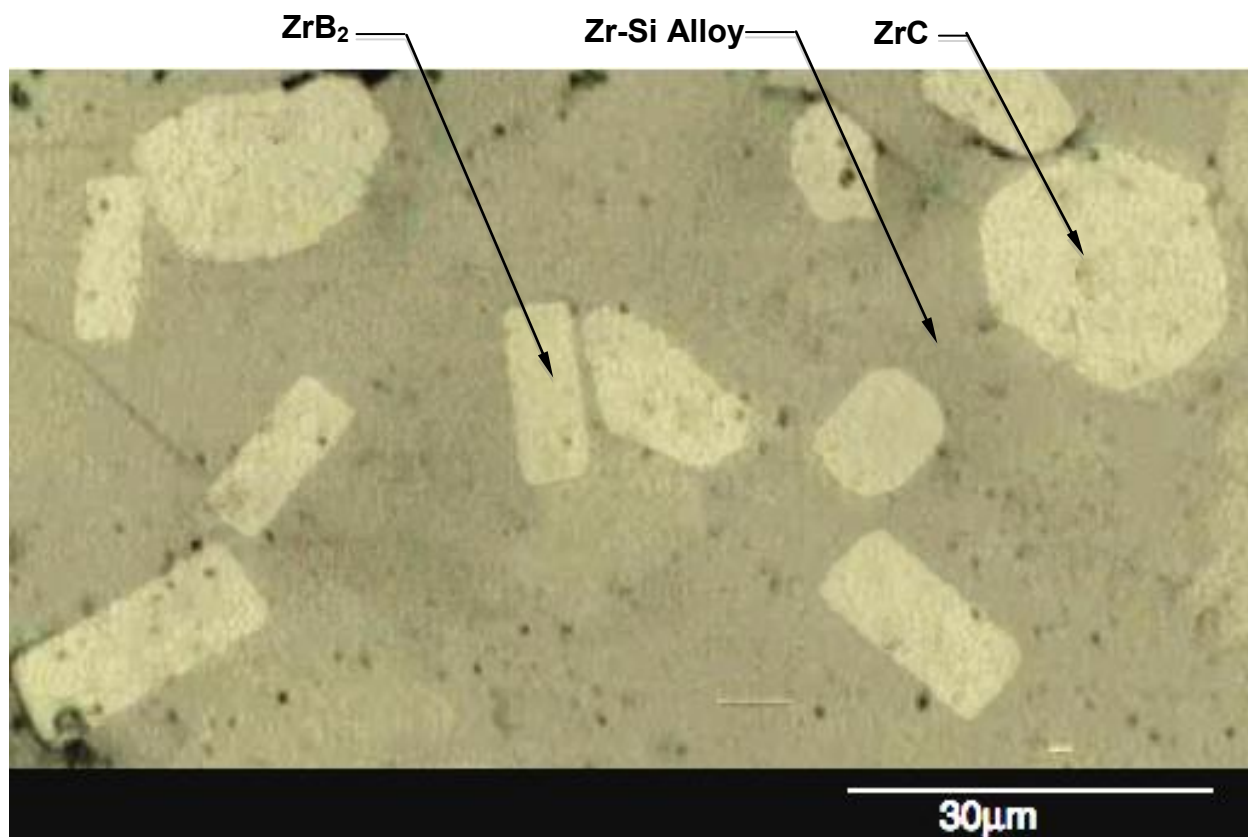


Figure 4.17: Micrograph with ZrB₂-ZrC precipitates in a completely reacted sample held at 1860°C for 240 minutes.

Chapter 5: DISCUSSION

5.1: Oxygen Potential Reduction within the graphite Enclosure

The absence of ZrO_2 and Al_2O_3 peaks in the x-ray diffraction patterns shown from figure 4.2 to figure 4.9, for the 2 different compositions of samples processed for 60 to 240 minutes indicate successful reduction of the oxygen potential within the graphite enclosure by the aluminum and titanium slugs. The removal of oxygen can be explained with the help of the Ellingham diagram, which depicts Gibbs free energy of formation with temperature. The Ellingham diagram for the oxides (figure 5.1) indicates that at 2000 °C, Y_2O_3 is the most stable oxide, as demonstrated by the lowest free energy. For ZrO_2 and Al_2O_3 , the lines intersect at 730°C, which suggests that at temperatures less than 730°C, the liquid aluminum (melting temperature of 665°C) has greater affinity for oxygen than zirconium does.

5.2: Phase Relations between Zr/B₄C/Si

The Zr-B₄C-ZrSi₂ ternary phase diagram at 1900°C and 2400°C shown in figures 5.2 and 5.3, respectively, suggests the formation of solid ZrB_2 and ZrC with liquid for the chosen stoichiometric ratios of Zr-12wt%Si (blue line) and Zr-16wt%Si (red line). The isothermal section of the phase diagram is observed at 2400 °C also, to account for the temperature rise inside the graphite crucible due to the highly exothermic nature of the reactions. Johnson et al. [6] reported adiabatic reaction temperatures to reach around 2300 °C-2400°C during the processing of ZrB_2 -ZrC-Zr composites. Three zirconium silicides, $ZrSi$, Zr_2Si and Zr_5Si_3 are observed in the phase

diagrams. The compound SiB_{14} , formed by the reaction between B_4C and SiB_6 , decomposes before 2400°C is reached and was never observed on the XRD patterns.

5.3: X-Ray Diffraction

The XRD spectrums (figures 4.2 to 4.9) for the samples reacted for 60, 120, 180, and 240 minutes, indicates the formation of ZrB_2 and ZrC precipitates in a solidified Zr-Si melt. ZrSi , is the only silicide to make an appearance in XRD spectrums for all the samples. This suggests the ZrSi prevails over all other silicides to become the main silicide. There was no considerable difference observed in the phases detected for the 2 different stoichiometric ratios due its closeness on the Zr-Si phase diagram [6]. The formation of ZrSi means the reaction moved to the left of Zr_3Si on the Zr-Si phase diagram shown in figure 2.1. To understand the formation of Zr_5Si_4 in all the samples except for samples reacted for 60 minutes, Ellingham diagrams for silicides are plotted. The Gibbs free energy of formation for the different silicides was generated using FactSage. Table 5.1 shows the Gibbs free energy of formation at temperatures, 200°C , 800°C , 1500°C , 2000°C , and 2500°C . In the plot of ΔG vs. temperature (figure 5.4), Zr_5Si_4 is the most stable silicide, which explains its presence in the XRD results. Zr_5Si_3 is the second most stable silicide, which is a discrepancy due its metastable nature at temperatures lower than 1745°C , which is not available on the FactSage database. The formation of Zr_2Si in the Zr-16wt\%Si sample reacted for 240 minutes is probably due to separate magnetic field mixing or kinetic problem with the reaction not proceeding to form Zr-Si or Zr_5Si_4 .

5.4: Microstructures

The microstructure images for the samples reacted for 60, 120, 180, and 240 minutes are shown from figures 4.10 to 4.17. The microstructures obtained are as suggested by the phase diagram with ZrB_2 and ZrC precipitates dispersed in solidified liquid. There was considerable unreacted B_4C in the 60 minutes and 120 minutes samples. This is a result of insufficient time for the reactants to achieve thermochemical equilibria as a more continuous microstructures with little unreacted B_4C were observed in the 180 minutes and 240 minutes samples. The formation of ZrB_2 and ZrC surrounded by solidified Zr-Si melt is due to the melting of zirconium slugs to form Zr-Si melt which reacts with B_4C to form ZrB_2 and ZrC . On a Zr-B-C ternary, the join representing the Zr liquid reacting with B_4C is shown in figure 2.4. Through the mass balance, the ZrC and ZrB_2 are formed as necessitated by the diffusional path crossing the join at least once, The shaded areas on either side of the join must be equal. Zr_5Si_3 appears in the Zr- B_4C -Si ternary phase diagram but is not seen in the samples due to its metastable state at lower temperatures [Okamoto-1990].

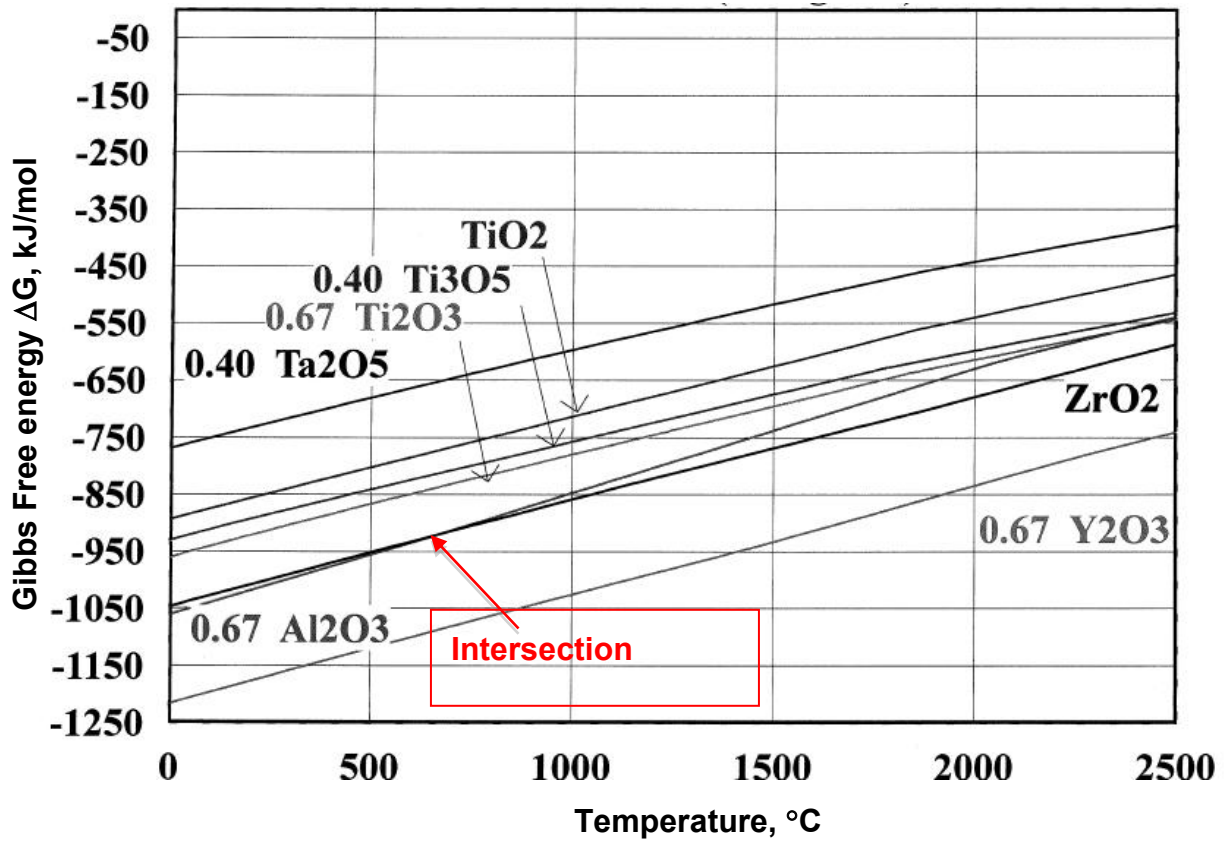


Figure 5.1: Ellingham Diagram for oxides.

Zr - B₄C - Si

2163 K

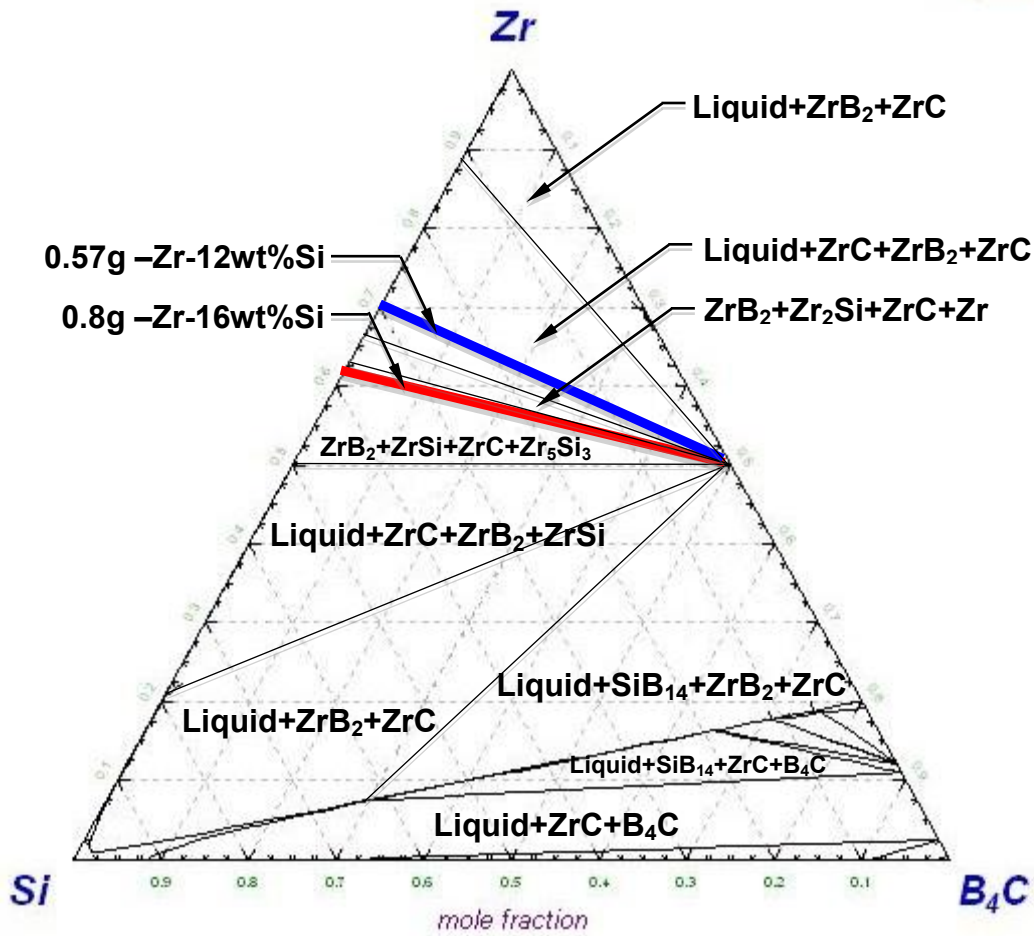


Figure 5.2: Zr-B₄C-Si Pseudo-Ternary Phase Diagram at 1900°C.

Zr - B₄C - Si

2673 K



Zr

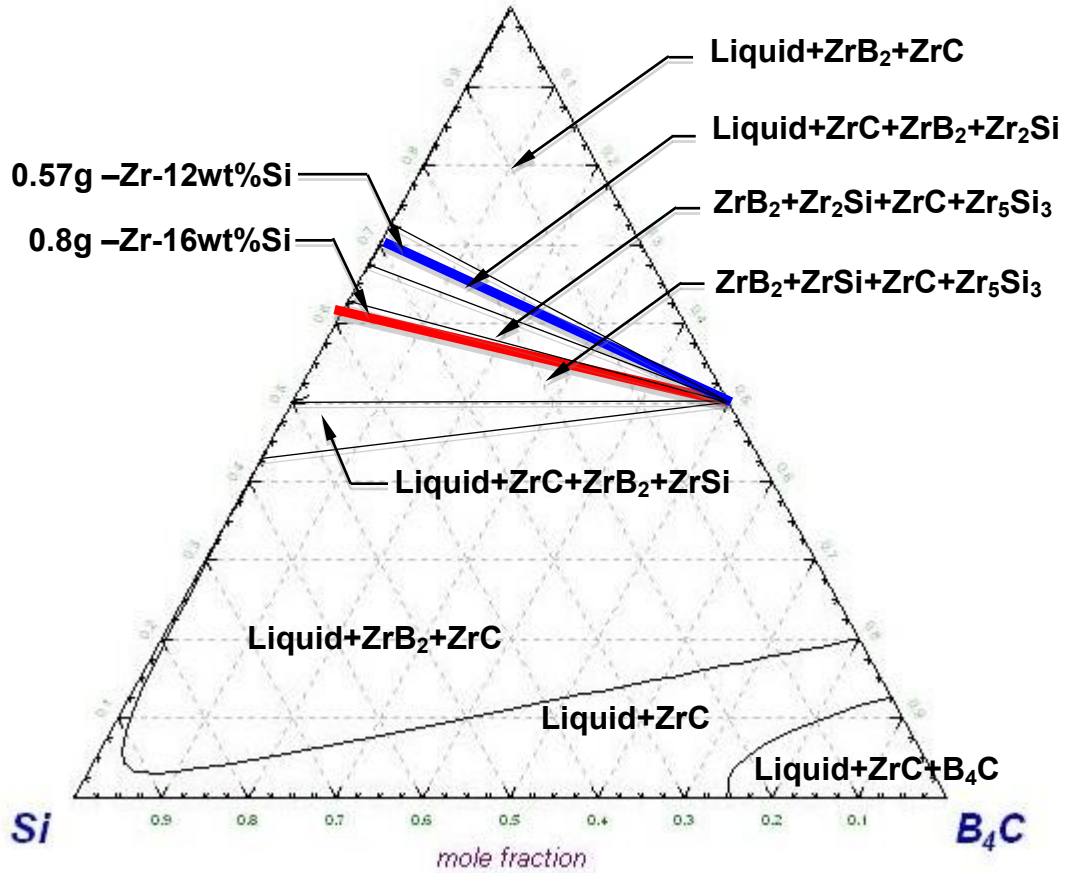


Figure 5.3: Zr-B₄C-Si Pseudo-Ternary Phase Diagram at 2400°C.

Table 5.1 Gibbs free energy of formation for zirconium silicides.

Temperature °C	Zr ₃ Si kJ/mol	Zr ₂ Si kJ/mol	Zr ₃ Si ₂ kJ/mol	Zr ₅ Si ₄ kJ/mol	ZrSi kJ/mol	ZrSi ₂ kJ/mol
200	-231	-223	-422.	-763	-163	-168
800	-214	-210	-395	-721	-155	-163
1500	-188	-199	-351	-648	-145	-149
2000	-156	-175	-289	-534	-124	-111

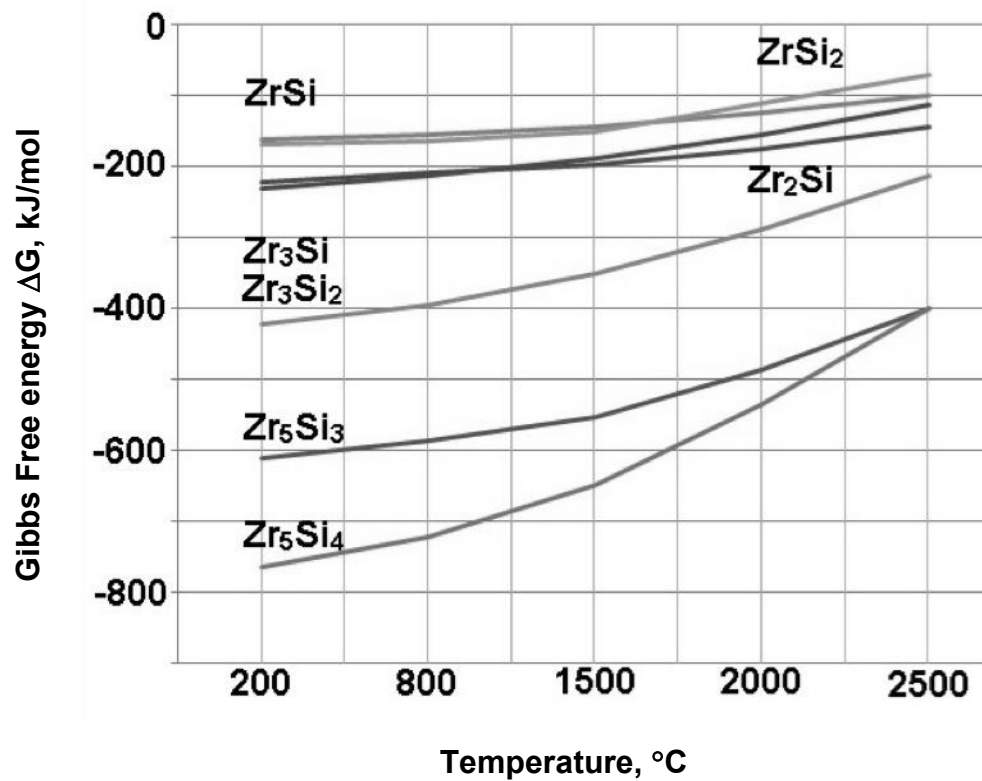


Figure 5.4: Ellingham Diagram for Zirconium Silicides.

Chapter 6: CONCLUSION

Two compositions of stoichiometric ratios, Zr-12wt%Si and Zr-16wt%Si, were reacted with B_4C at 1860 °C for 60 minutes, 120, 180, and 240 to determine the relationship between time and reactivity. The processed samples were characterized using an optical microscope and x-ray diffraction (XRD). Microstructures with ZrB_2 and ZrC precipitates surrounded by solidified Zr-Si melt were observed in all the samples as expected with ZrSi, the main phase of silicide detected. Free B_4C was detected in the 60 minutes and 120 minutes due to short duration of reaction time. One concern was the considerable porosity observed due to the furnace's electromagnetic field, which levitated the Zr liquid, but the ZrO_2 - Y_2O_3 crucible shield decreased the levitation significantly. The Zr-Si liquid reacted completely with B_4C as observed in the 180 minutes and 240 minutes samples suggesting sufficient time for the reactants to attain phase equilibria was reached for the ultrahigh temperatures achieved.

REFERENCES

- [1] Bronson, A., Ma, Yu-Tao., Mutso, R. R., and Pingitore, N., Compatibility of refractory metal boride/oxide composites at ultrahigh temperatures. *Journal of Electrochemical Society.*, 1992, 139(11), 3183-3196.
- [2] Bronson, A. and Odegard, C., The reactive liquid processing of ceramic -metal composites. *Journal of the Minerals, Metals & Materials Society*, 1997, 52-54.
- [3] Bronson, A., and Chessa, J., Evaluation of vaporizing rates of SiO₂ and TiO₂ as protective coatings for ultrahigh temperature ceramic composites. *Journal of European Ceramic Society*, 2008, 91(5), 1448-1452.
- [4] Canel, J., Zaman, J., Bettembourg, J., Flem, M. L. and Poissonnet, S., Composite zirconium silicides through an in situ process. *International Journal of Applied Ceramic Technology.*, 2006, 3(1), 23-31.
- [5] FactSage, Company: Thermfact/ CRCT-GTT, File version 6.1.
- [6] Fahrenholtz, W. G., Reactive Processing in Ceramic -Based Systems. *International Journal of Applied Ceramic Technology*, 2006, 3(1), 1-12.
- [7] Fahrenholtz, W. G., Hilmas, G. E., Refractory Diborides of Zirconium and Hafnium. *J. American Ceramic Society*, 2007, 90(5), 1347-1364.
- [8] Fahrenholtz, W. G., Rezaie, A., and Hilmas, G. E., Evolution of structure during the oxidation of zirconium diboride -silicon carbide in air up to 1500 °C. *Journal of American Ceramic Society*, 2007, 27, 2495-2501.

- [9] Hinze, J. W., Tripp, W. C. and Graham, H. C., The high -temperature oxidation behavior of a HfB₂+20 v/o SiC composite. Journal of Electrochemical Society, 1975, 122(9), 1249-1254.
- [10] Johnson, W. B., Nagalberg, A. S. and Breval, E., Kinetics of formation of a platelet - reinforced ceramic composite prepared by a directed reaction of zirconium with boron carbide. Journal of American Ceramic Society, 1991, 74(9), 2093-2101.
- [11] Kaiser, A., Lobert, M., and Telle, R, Thermal stability of zircon (ZrSiO₄). Journal of European Ceramic Society, 2008, 28, 2199-2211.
- [12] Karlsdottir, S. N., and Halloran, J. W., Rapid oxidation characterization of ultra -high temperature ceramics, Journal of American Ceramic Society, 2007, 92(2), 481-486.
- [13] Levine, S. R., Opila, E. J., Halbig, M. C., Kiser, J. D., Singh, M., and Salem, J. A., Evaluation of ultra -high temperature ceramics for aeropropulsion use. Journal of European Ceramic Society, 2002, 22, 2757-2767.
- [14] Lu, P. and Du, T. B. and Loehman, R. E., Ewsuk, K. G. and Fahrenholtz, W. G., Interfacial microstructure formed by reactive metal penetration of Al into mullite. Journal of Materials Research, 1999, 14(9), 3530-3537.
- [15] Monteverde, F., and Savino, R., Stability of ultra -high-temperature ZrB₂ -SiC ceramics under simulated atmospheric re -entry conditions. Journal of European Ceramic Society, 2007, 27, 4797-4805.
- [16] Okamoto, H., the Si-Zr System. ASM International, 1990, 11(5), 513-519.
- [17] Okamoto, H., B -Zr (Boron -Zirconium). Journal of Phase Equilibria, 1993, 14(2), 261-262.

- [18] Okamoto, H., C -Zr (Carbon -Zirconium). Journal of Phase Equilibria, 1996, 17(2), 162.
- [19] Opeka, M. M., Talmy, I. G. and Zaykoski, J. A., Oxidation-based materials selection for 2000°C+ hypersonic aerosurfaces: theoretical considerations and historical experience. Journal of Materials Science, 2004, 39(19), 5887-5904.
- [20] Outotec
- [21] Petla, H., Renova, E. P., Bronson, A., Chessa, J. F., and Maheswar aiah, B. M., A computational analysis of a ZrO_2 - SiO_2 scale for a ZrB_2 -ZrC-Zr ultrahigh temperature ceramic composite system. Journal of European Ceramic Society, 2010.
- [22] Sorrell, C. C., McCartney, E. R., Phase equilibrium in the system zirconium-silicon-oxygen. In: Proceedings of the 12th Australian Ceramics Conference, 1986.
- [23] Tomsia, A. P., Saiz, E., Foppiano, S., MoberlyChan, W., Synthesis and processing of ceramic-metal composites by reactive metal penetration. Composites: Part A, 1999, 30, 399-403.

CURRICULUM VITA

Nischel B. Maheswaraiah was born on July 2, 1985, in Shimoga, Karnataka, India. The second son of Maheswaraiah Shivanna and Bhagyavathi Basappa, he graduated with Mathematics and Science Degree in 2003 from Karnataka Lingayat Education College (Bangalore, India). He received his Bachelor's degree in Mechanical Engineering from People's Education Society Institute of Technology (P.E.S.I.T) in 2007. He finished his Master's in Mechanical Engineering in 2010 at University of Texas at El Paso, El Paso, Texas.

Permanent address: 178, Shankarnagar

Bangalore – 560096

India

This Thesis was typed by Nischel B. Maheswaraiah